In situ gelling implants based on temperature-responsive amphiphilic triblock copolymers

Master thesis in Pharmaceutics

Josefine Eilsø Nielsen

Department of Chemistry

Department of Pharmacy, School of Pharmacy

The Faculty of Mathematics and Natural Sciences

UNIVERSITY OF OSLO

May 2015

In situ gelling implants based on temperature-responsive amphiphilic triblock copolymers

by

Josefine Eilsø Nielsen

Supervisors:

Professor Sverre Arne Sande

Professor Bo Nyström

Department of Chemistry

Department of Pharmacy, School of Pharmacy

THE FACUTLY OF MATHEMATICS AND NATURAL SCIENCE

UNIVERSITY OF OSLO

May 2015

Year 2015

In situ gelling implants based on temperature-responsive amphiphilic triblock copolymers

Josefine Eilsø Nielsen

http://www.duo.uio.no/

Printed at Reprosentralen, Universitetet i Oslo

Abstract

In this thesis, emphasis is given to the study of temperature-responsive amphiphilic triblock copolymers and their use for *in situ* drug delivery systems. Two polymers have been studied with approximately the same composition of the two hydrophobic caprolactone copolymerised with lactic acid (PCLA) end groups. The middle hydrophilic poly(ethylene glycol) (PEG) spacer is different between the polymers; respectively with a molecular weight of 1000 and 1500 g/mol. PCLA-PEG-PCLA is showed to form a gel that is temperature dependent.

The polymeric systems were characterised in terms of their rheological properties through laboratory measurements, i.e. gel point, dynamic viscosity, gel properties and thermodynamic features in form of cloud point. It was proven that both the concentration and length of the hydrophilic PEG spacer affects the rheology and structure of the system. A sol-gel-sol (phase separation) transition was observed for both polymer systems via the tube inverting method. It was only possible to determine a critical gel point for the PCLA-PEG(1000)-PCLA polymer.

The properties of the polymer with the short PEG spacer, observed from small angle neutron scattering measurements, could be explained by formation of worm-like cylindrical micelles. The polymer with the longer PEG spacer forms flower-like spherical core-shell micelles. It was shown through rheology tests that these cylinders were less stable upon heating and therefore more temperature-responsive.

Acknowledgement

The present work was performed at the Department of Chemistry and at the Department of Pharmacy at the University of Oslo, for the master degree in Pharmacy at School of Pharmacy, at the University of Oslo in the period August 2014 to May 2015.

First of all, I would like to thank my two supervisor's prof. Bo Nyström and Prof. Sverre Arne Sande whose guidance and support has been essential for the completion of this thesis. I have greatly valued their encouragement, advice and constructive comments.

I am grateful to Prof. Kenneth Knudsen at the Institute for Energy Technology for his help with performing and analysing small angle neutron scattering experiments. Being able to disscuss my results with you have been essential for my work. I would also like to thank Dr. Kaizheng Zhu for synthesising the polymers which are studied in this thesis.Thanks to Tove Larsen at the Department of Pharmacy for technical support.

Special thanks go to Dr. Thomas Zinn for helping me with rheology (and much more), and to Dr. Reidar Lund for helping me with SANS fitting. I have especially valued how both of you always take the time to answer my questions even at stressful moments.

I am very grateful to everyone in the research group at the Department of Chemistry for all your support, and for making this period great fun.

During my five years of studies I have met some fantastic people, you know who you are. Without you these five years would not be at least as fun as they have been. I deeply value your friendship!

Finally I would like to thank my parents because they always support me in everything I do. From you I have inherited the passion for science, and for this I am profoundly grateful.

Josefine Eilsø Nielsen

May, 2015

Abbreviations

°C	Degrees Celsius
2Θ	Scattering angle
C*	Critical concentration for overlapping polymers in solution
CL	Caprolactone
CP	Cloud point
DLS	dynamic light scattering
DSC	Differential Scanning Calorimeter
EHEC	Ethyl(hydroxyethyl)cellulose
FDA	U S Food and Drug Administration
G*	Complex modulus
G’	Storage modulus
G’’	Loss modulus
GP	Gel point
I(q)	Scattering intensity
LA	Lactic acid
LCST	Lower critical solution temperature
LVE range	Linear viscoelastic range
n	The relaxation exponent
n’, n’’	The viscoelastic exponents ($G' \sim \omega^{n'}$; $G'' \sim \omega^{n''}$)

P(q)	Form factor
PCL	Poly(caprolactone)
PCLA	Poly(caprolacton-co-lactic acid)
PEG	Poly(ethylene glycol)
PEO	Poly(oxyethylene)
PLA	Poly(lactic acid)
PLGA	Poly(lactic-co-glycolic acid)
PPO	Poly(propylene oxide)
PVA	Poly(vinyl alcohol)
q	scattering vector
Rm	Radius of micelle
S	Gel-strength
S(q)	Structure factor
SANS	Small angle neutron scattering
SDS	Sodium dodecyl sulphate
t	Time
tan δ	Loss or damping tangent
T_m	Melting temperature
UCST	Upper critical solution temperature
wt%	Weight percent
γ	Strain amplitude

η'	The dynamic viscosity
σ	Shear stress
ω	Angular frequency in s^{-1}

Table of contents:

1 Introduction

The end objective of the naltrexone-project is to investigate an injectable formulation of naltrexone based on a temperature-responsive triblock copolymer. The hypothesis is that this polymer will undergo a phase transition from solution to gel network *in situ* (Figure 1).

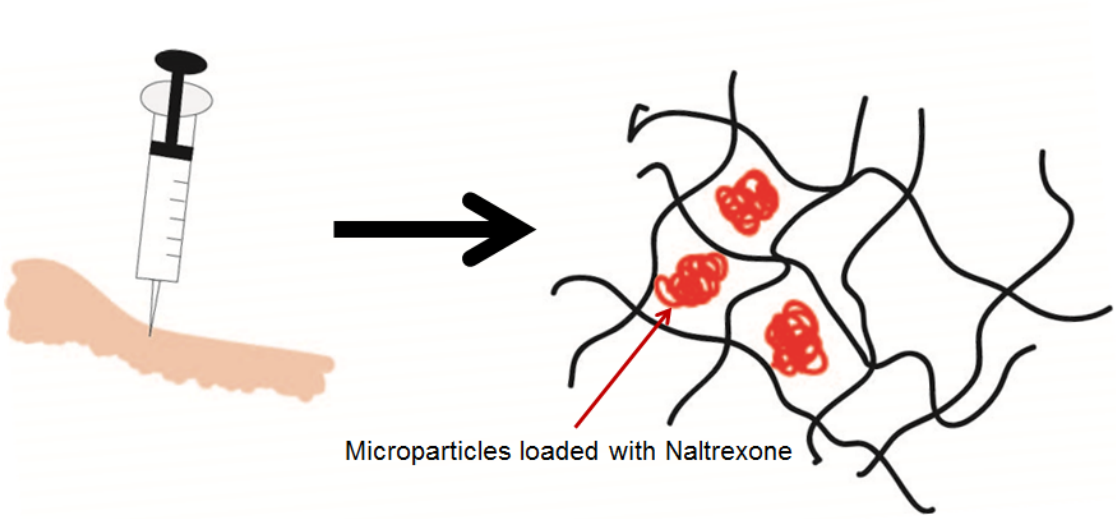

Figure 1. Illustration of a drug formulation which undergoes gelation after being injected into the patient.

Naltrexone acts as an opioid antagonist by blocking the μ- receptor as seen in Figure 2. A long lasting depot formulation of Naltrexone can therefore be used to treat opiate addiction. The Norwegian Institute of Public Health preformed a study in 2003 were they used Naltrexone implants to treat ten heroin-dependent patients. In this study solid Naltrexone implants was surgically implanted under the skin of the patients. In the paper written by L. Olsen et al. they concluded that Naltrexone implants provide protective plasma drug concentrations during prolonged periods of treatment. The implant was in general well tolerated, but 2 of the 10 patients developed tissue reactions after repeated implantation. L. Olsen et al. discussed that these reactions may be specific to the depot formulation used because naltrexone is not known to cause such reactions. They suggested that other depot formulations should be evaluated [1]. We believe that a polymer-based formulation that can be injected in the liquid phase, for then to undergo gelation at body temperature will solve the problems identified by L. Olsen et al.

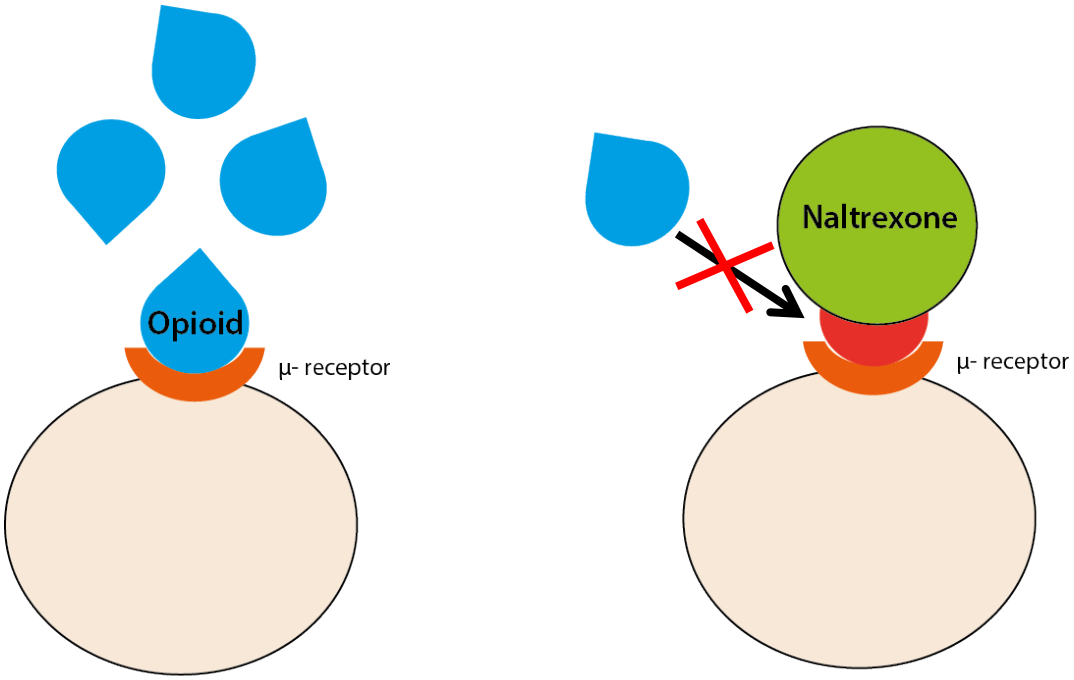

Figure 2. Sketch of how the naltrexone drug blocks the μ-receptor.

To achieve controlled release from the gel network it has been suggested to incorporate drug loaded polymer-based microparticles (as seen in Figure 1). They will enhance the stability of the formulation and reduce burst release of drug from the formulation [2]. The purpose of the gel matrix is to retain the particles in the refined compartment. The purpose of this master project was to find a suitable polymer for the *in situ* gelling drug delivery system.

Choosing the appropriate polymer system for the gel matrix has proven to be a challenge. The first option that has been investigated is poly(oxyethylene)-b-poly(oxypropylene)-b-poly(oxyethylene) (PEO-PPO-PEO) also known as Pluronic. This polymer has been widely studied because of its temperature responsive properties. This system has proven to be too soluble because the PPO is not sufficiently hydrophobic. This causes the gel to degrade too quickly in the body. A.L. Kjøniksen et al. tried to modify Pluronic with HEC [3] and polysaccharides [4] to increase the stability of the hydrogel. In this study they managed to decrease the dissolution rate, but the system still degraded to fast to act as a sustained release formulation over a sufficient period of time.

An alternative system was investigated by M. T. Calejo et al. [5-7] based on the combination of ethyl/hydroxyethyl) cellulose (EHEC) and amino acid containing surfactants. This system

has proven to be complex; the gelation is strongly dependent on the concentration of surfactants. A high amount of surfactants are shown to have some cytotoxicity. The EHEC system showed some promising properties in water, but in a body like environment the complexity of the EHEC system is not ideal as a gel matrix for drug delivery.

The idea of using a polymer consisting of two hydrophobic blocks with a middle hydrophilic spacer could be a solution to the problems observed in the earlier studies. This polymer would be more hydrophobic and therefor supposedly be degrading at a lower rate. A promising candidate for this purpose is the amphiphilic temperature-responsive triblock copolymer: PCLA-PEG-PCLA.

The properties of the gel system need to be investigated fully to decide if PCLA-PEG-PCLA is the ideal gel matrix for a sustained release Naltrexone formulation. In this project the polymer has been investigated by combining results from rheology, turbidity and small angle scattering techniques. We wanted to see how the properties of the polymer evolve with alterations in temperature, length of PEG spacer and concentration. From this information we can understand how to design, and control, the properties of this polymeric system to achieve the ideal controlled drug delivery formulation.

2 Theory and background

2.1 Drug Delivery

Drugs can be delivered to the patient in different dosage forms and for different routes as seen in Table 1. In which form the drug may be administered or by which route depends on different factors like for example the age of the patient, the half-life of the drug substance, and toxicity when exposed to the systemic route. The objective of dosage form design is to achieve predictable therapeutic response to a given drug [8].

Table 1. Table of dosage forms available for different administration routes based on Table 1.1 in Aulton's book of Pharmaceutics.[8]

Administration route	**Dosage forms**
Oral	Solutions, suspensions, emulsions, gels, powders, granules, capsules, tablets
Rectal/ vaginal	Suppositories, ointments, creams, powders, solutions
Topical	Ointments, creams, lotions, gels, solutions, topical aerosols, transdermal patches
Parenteral	Injections (solution, suspension, emulsion forms), implants,
Respiratory	Aerosols (solution, suspension, emulsion, powder forms), gases
Nasal	Solutions
Eye	Solutions, ointments, creams
Ear	Solutions, suspensions, ointments, creams

Research into improving the safety-efficacy ratio of existing drugs is a lucrative alternative to development of new drug molecules. This is because the development of new drug molecules is both expensive and time consuming. Improving the therapy from existing drugs may be obtained by methods like individualising drug therapy, therapeutic drug monitoring and dose titrations. An alternative and very attractive method is the application of controlled drug delivery formulations for these drugs. Here we can deliver the drug at controlled rate, depot delivery over a long time, and target the delivery to a specific site [9]. By using controlled drug delivery systems, we can achieve lower toxicity for the patient and improve the adherence by making it more practical for the patient to take the drug.

An *in situ* gelling drug delivery system does not fit into the traditional classification of dosage forms. The formulation can both be classified as an injectable solution, suspension and as an implant.

Stimuli responsive polymer has been suggested as an interesting excipient for drug delivery formulations [10, 11]. This is further elaborated in the next paragraphs.

2.2 Stimuli responsive polymers

Polymers that undergo relatively large and abrupt, physical or chemical changes in response to small external changes are classified as stimuli responsive polymers. The stimuli can be divided into chemical and physical stimuli. Classical examples of chemical stimuli are addition of chemical agents, pH changes and ionic strength variation. These chemical stimuli will affect the system at a molecular level. They can modulate the interactions between polymer chains and the solvent, or between the chains themselves. On the other hand, physical stimuli will alter molecular interactions at critical onset points. Typical examples of physical stimuli are temperature changes, mechanical stress and electric or magnetic field variation [11].

Some polysaccharides, proteins and nucleic acids are examples of stimuli-responsive polymers. Such polymers are commonly found in living organisms. It is also possible to introduce stimuli-responsive polymers into a block copolymer architecture [11]. The numerous possibilities in designing stimuli-responsive block copolymers make it a very good candidate for controlled drug delivery formulation.

2.2.1 Temperature-responsive block copolymers

Temperature-responsive polymers exhibit either a lower critical solution temperature (LCST) or an upper critical solution temperature (UCST). Blocks exhibiting these properties can be incorporated into block copolymers. By doing this one can achieve for example temperature responsive micelle formation [11]. From Figure 3 one can see an example of a phase diagram for PEO with different molecular weights from a paper by E. Dormidontova. In this diagram we observe that PEO both has a lower and an upper critical solution temperature. We see that an increase in molecular weight leads to a lowered LCST and a corresponding rise in UCST. This behaviour is typical for polymer systems that exhibit hydrogen bonding. In contrast to normal polymer behaviour in which solubility increases with temperature, the solubility of these polymers decreases. This leads to phase separation above a critical temperature (LCST) that depends on the molecular weight of the polymer. At even higher temperatures (above UCST) the homogenous state becomes stable again. Formation of closed loop regions of phase coexistence is characteristic features for these polymers [12].

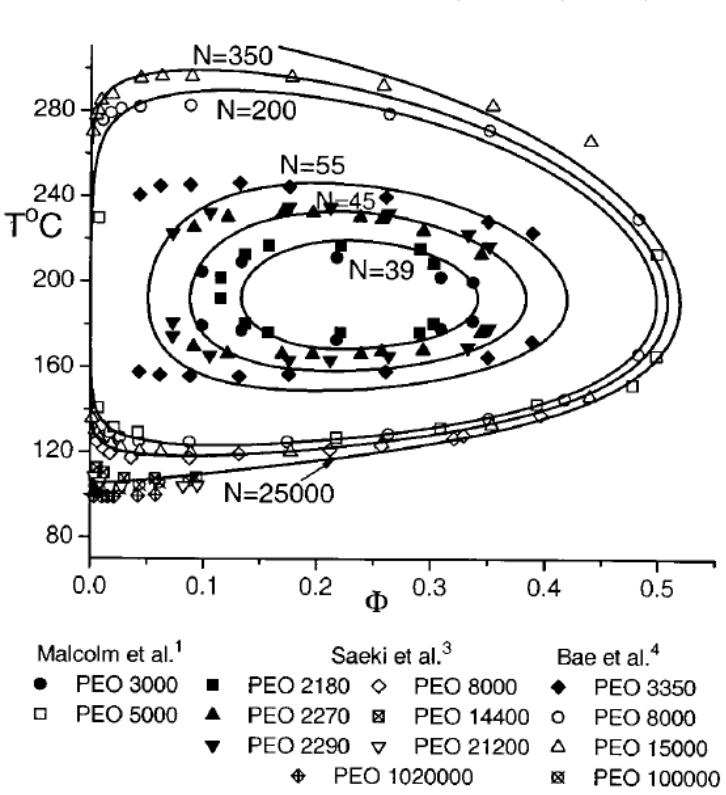

Figure 3. Phase diagram for aqueous solutions of PEO published by E. Dormidontova [12]. Here experimental data are represented by symbols and theoretical curves shown with solid lines. On the Y-axis we find the temperature in Celsius and on the X-axis the volume fraction (Φ). We see from this that PEO has both a lower and an upper critical solution temperature.

There has been extensive research into the use of temperature-responsive block copolymers as excipients in controlled drug delivery formulations. These polymers can for example be used to make temperature responsive hydrogels as is further discussed in paragraph 2.4.

Poly(ethylene glycol)

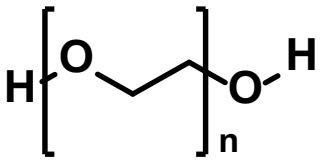

Figure 4. Molecular structure of PEG where n represents the number of monomer units.

Poly(ethylene glycol) (PEG) is an uncharged, hydrophilic and linear polymer (Figure 4). It is available commercially in a number of molecular weights. PEG is otherwise known as poly(ethylene oxide) (PEO) when the molecular weight of the polymer is high. PEG has both an upper and a lower critical solution temperature as described in paragraph 2.2.1, and shown

in Figure 3. Because of this feature PEG is often incorporated as the hydrophilic block in temperature-responsive amphiphilic block copolymers. One example of a temperature-responsive amphiphilic block copolymer is the commercially available product Pluronic. Pluronic is a triblock with two PEO blocks. In between the two PEO block there is a more hydrophobic poly(oxypropylene) block (PPO). Pluronic can form micelles [11] or polymeric gel networks [13] depending on concentration and molecular weights.

PEG is considered as a biocompatible polymer. It has a very low order of toxicity and is non-immunogenic. PEG is approved by the FDA for use as excipients or as a carrier in different pharmaceutical formulations, foods, and cosmetics [14]. The PEG polymer inhibits protein adsorption. They prolong the circulation time of particulate drug delivery systems, such as nanoparticles, through their adsorption or incorporation into the surface of the carriers. In this way they prevent the adsorption of opsonins and reduce the uptake by the liver and spleen [15]. These features make PEG a very interesting excipient in drug delivery formulations. One common example is the application of PEGylation of peptides and proteins to prolong the half time of these molecules [14, 15].

Poly(caprolactone)

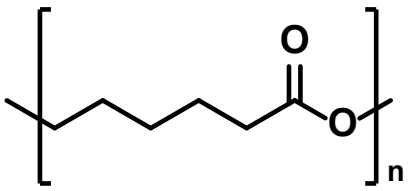

Figure 5. Molecular structure of PCL where n represents the number of monomer units.

Poly(caprolactone) (PCL) is linear aliphatic polyester (Figure 5). It has hydrophobic properties, and is 50 % crystalline [16]. Because of its crystalline nature it exhibits brittle properties instead of having the sticky paste morphology [17]. This is a convenient property of PCL if it is to be used in a full-scale industrial production of for example Pharmaceutical products. Crystalline polymers are easier to weigh and transfer because they have better flowing abilities. Their polymer morphology is dependent on temperature, and will have a melting point where it changes to a sticky high viscous liquid.

PCL is a biodegradable polymer. The polymer backbone is hydrolysable at the ester linkages [16].

PCL has been combined with a hydrophilic block of PEG either as PCL-PEG-PCL [17, 18] or PEG-PCL-PEG or MPEG-PCL [18] to form thermogels. One of the problems with these polymer systems is that because of PCL's crystalline properties the polymers easily precipitate.

Poly(lactic acid)

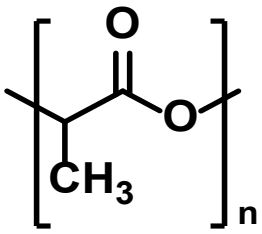

Figure 6. Molecular structure of PLA where n represents the number of monomer units.

Poly(lactic acid) (PLA) is another linear aliphatic polyester (Figure 6). It is a biodegradable polymer that is degraded via simple hydrolysis of the ester bonds and is not dependent on enzymes to catalyse the hydrolysis. PLA exist both on an L- and a D- form [19].

Lactic acid (LA) has been copolymerised with glycolic acid (GA) to form PLGA [18] or with Caprolactone (CL) to form PCLA [18, 20-23]. LA blocks the crystalline features of the polymer it is copolymerised with. This will therefore make it easier to dissolve the block copolymer in water. This has been proven by doing DSC measurements on bulk of PCLA-PEG-PCLA, PCL-PEG-PCL and PLA-PEG-PLA by Z. Zhang et al. In Figure 7 the thermogram for the tree polymers is shown. The polymer with only PEG and PCL has a clear endothermic peak (melting peak) upon heating and an exothermic peak (crystallisation peak) upon cooling. This indicates a crystalline morphology. A similar peak was not observed for the polymer with PLA as the hydrophobic block, or in the polymer with copolymerised LA and CL [20]. The dissolution power of these polymers is also dependent on the length of the hydrophilic PEG-spacer.

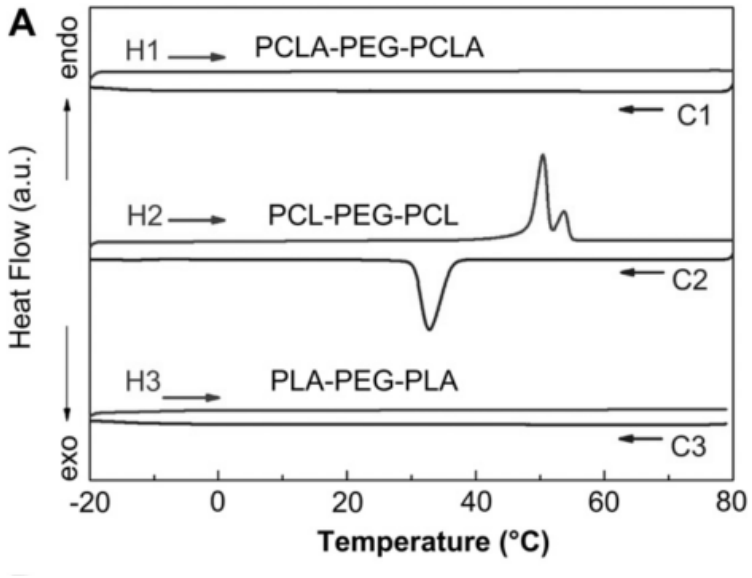

Figure 7. DSC thermograms published by Z. Zang et al. of the indicated triblock copolymers. The heating and cooling rate was 5 °C/min. H1, H2, H3 are heating curves, while C1, C2, C3 are cooling curves [20].

2.2.2 Polymer solutions

Polymer solutions are liquid mixtures of long polymer chains and small, light solvent molecules. The solvent can for example be pure water or a buffer solution. In a dilute polymer solution, the polymer coils act as independent units, whereas at higher concentrations the coils start to overlap at the crossover concentration c*. Above this concentration, in the semi dilute regime, a transient network is formed. At still higher concentrations we have a more or less homogeneous segment distribution and we enter the dense concentration regime. If the chains are sufficiently long we encounter a situation of entangled polymer chains (see Figure 8).

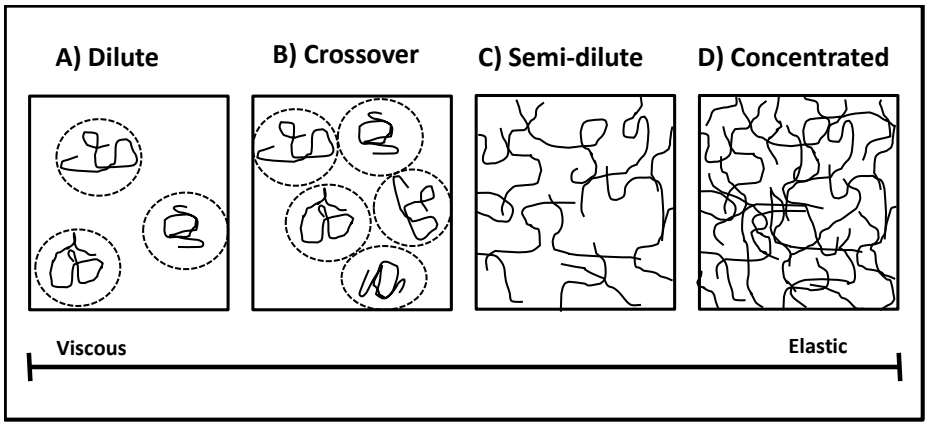

Figure 8. A sketch of concentration regimes of a polymer solution. A) Coils do not overlap c << c → dilute polymer solution; B) Coils are at the point of overlapping c ≈ c* → crossover between a dilute and semi-dilute polymer solution; C) Coils strongly overlap*

2.3 Self-assembling amphiphilic block copolymers

In a block copolymer each block generally maintains their specific properties while connected in a single polymer chain. An example is amphiphilic block copolymers that consist of both hydrophilic and hydrophobic blocks. Immiscibility between blocks often induces changes in the higher ordered structures. This will happen when amphiphilic block copolymers are introduced in a solvent (typically water). The polymers will then self-assemble into micelles as illustrated in Figure 9. The insoluble blocks form the micellar core and the soluble blocks constitute the corona. The size of these polymeric micelles often ranges from 20-100 nm [11]. These micelles are in dynamic equilibrium with free molecules in the solution, and will continuously break down and reform [15].

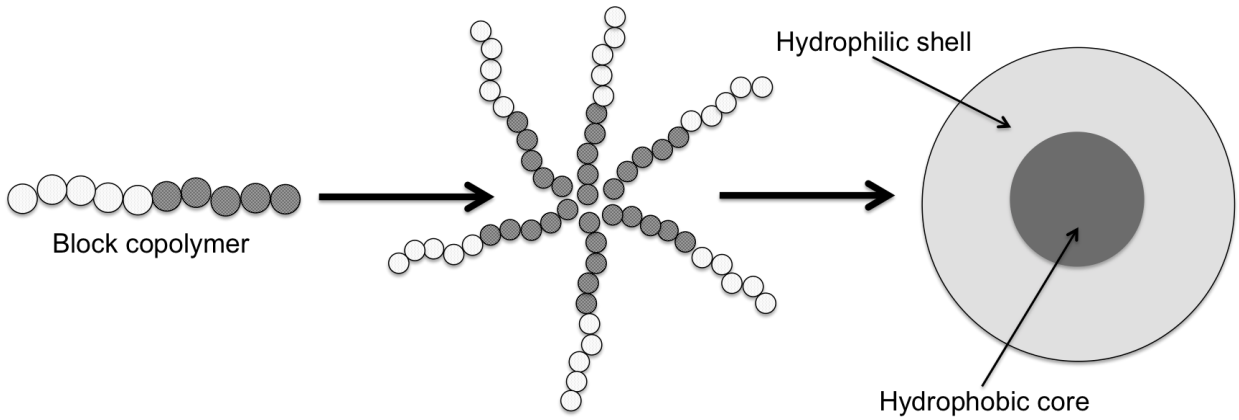

Figure 9. Illustration of how amphiphilic diblock copolymers self-assemble into polymeric micelles in water.

As described above, block copolymers can consist of one or several stimuli-responsive blocks. An amphiphilic diblock copolymer containing a hydrophobic block linked to a stimuli-responsive water-soluble block, will for example form a stimuli-responsive micelle in water. In this system the stimuli-responsive hydrophilic chains in the shell can become more hydrophobic because of stimuli. In the case of a temperature responsive polymer system the shell becomes dehydrated. This will lead to hydrophobization of the copolymer, and eventually precipitation or flocculation is observed [11].

Stimuli of block copolymer micelles can also cause morphological changes. This can result in the formation of rods, disks or vehicles. The morphology of micelles is also dependent on other parameters like concentration and the geometry of the polymer molecule (the packing

parameter) [15, 24]. The morphology of micelles can therefore be tuned by altering these different parameters.

The packing parameter was introduced by J. Israelchivili et al. as an important factor in the morphology of self-assembly surfactants [24].

$$P = \frac{V_0}{a_e I_0} \quad (1)$$

Here P is the packing parameter, V_0 is the tail volume (volume of the hydrophobic chain), I_0 is the tail length and a_e is the equilibrium area per molecule at the aggregate interface. The packing parameter relates to the geometrical structure as seen in Table 2 and illustrated in Figure 10.

Table 2. Prediction of the shape of self-assembled structures in solution based on the packing parameter [24].

	Sphere	Cylinder	Bilayer
Packing parameter	≤1/3	≤1/2	≤1

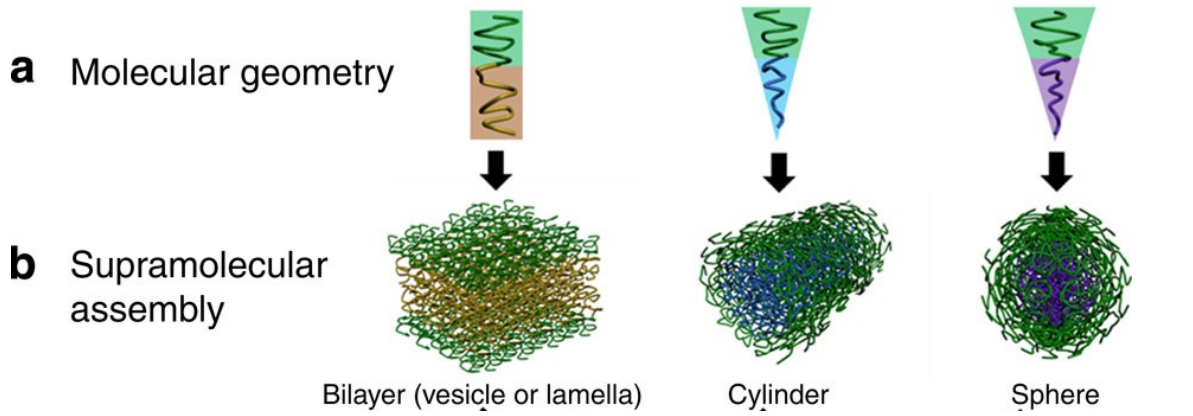

Figure 10 A) the molecular geometry related to the packing parameter. B) The resulting structure of the self-assemblies in solution [25].

Micelles are popular candidates as controlled drug delivery matrixes. Water-insoluble drugs can be incorporated into the core of the hydrophobic core of the micelles. This process, whereby water-insoluble drugs are brought into solution, is termed solubilisation [15]. Another advantage in using micelles for drug delivery is the fact that the micelles are small. They can be used as nanocarriers to specific targets in the body, for example transporting anticancer drugs to solid tumours [11].

2.4 Temperature-responsive polymeric hydrogels

Hydrogels are three-dimensional network structures obtained from a class of natural and/or synthetic polymers which absorb and retain large amounts of water (from 10% and up to thousands of times their dry weight). When hydrated in an aqueous environment the hydrophilic groups, or domains present in the polymeric network, create the gel structure [26]. There are great structural similarities between hydrogels and the macromolecular-based components in the body. Many hydrogels are therefore considered to be biocompatible. This term relates to the hydrogel's ability to exist inside a human body without damaging cells, cause scarring or in other ways cause negative responses from the body [27].

Hydrogels can be divided into two main categories: physical gels and chemical gels. Chemical gels are non-reversible and are therefore also called permanent gels. These consist of covalently-crosslinked networks of polymers [28]. The gels formed in this manner are often much stronger than physical gels. In this paragraph I will focus on discussing physical gels because these often are temperature-responsive.

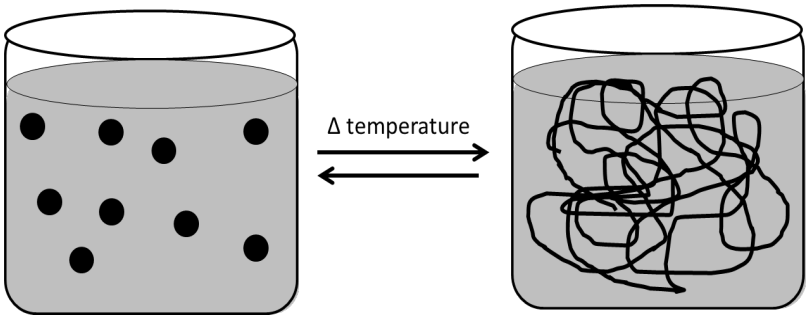

Figure 11. The sol to gel transition of a temperature responsive block copolymer in water

Physical gels are also called reversible gels, and this notation includes gel-networks held together by molecular entanglements, and/or secondary forces including ionic, hydrogen bonds and hydrophobic forces [28]. Physical gels can be heat reversible and has a transition from solution to gel either with heating or cooling [8] (Figure 11). Other physical gels may also respond to alterations in pH. A common example of a polymeric system that undergoes a phase transition from solution to gel with alterations in temperature is gelatine. A 1.5% solution of gelatine in water is, at high temperatures, a simple solution of chains (sol). If the temperature is decreased we get a gel network. When we reheat the system we recover the sol phase. However the transition temperature measured at heating is often higher than the

transition point measured on cooling. This is termed a hysteresis effect, and is caused by the complexity of the association processes that form the physical gel network [29].

The Nobel Prize winner in Physics of 1991, Pierre-Gilles de Gennes identified three types of interactions that can lead to physical gelation: local helical structures where one molecule winds around another, microcrystallites with partial alignment of the polymeric chains; and nodular domain, where the chains are heterogeneous and association only occurs at preferred sites along the chain. We can for example have this formation of nodules with triblock BAB-polymer. When it is dissolved in a solvent that is good for the A block and poor for B block, the B portion will tend to coalesce into nodules. We call these structures for micelles (as described further in detail in section 2.3) if this system is in the fluid state. Liquide nodules leads to a highly reversible sol-gel transition [29].

Temperature-responsive hydrogels can be used in controlled drug delivery. This can be accomplished by using a semi dilute aqueous solution, which undergoes a sol-to-gel transition within a certain temperature range [18]. In drug delivery, the most interesting thermogels are those that change from solution to gel within the physiologically relevant temperature range. There are many advantages with using thermogels in controlled drug delivery. It is relatively easy to incorporate the drug in the gel. To achieve this we mix the drug and polymer solution at a temperature below the gel point. Another advantage is that the drug system can be injected into the patient as a liquid. One can imagine that the polymer system undergoes a phase transition from sol to gel *in situ*. This will happen because of the increase in temperature from room temperature (or below) to body temperature. The polymeric gel system can work as a depot of medicine. The amount of drug released from the matrix and the velocity of the release can be adjusted by doing changes in the polymer system. Unlike solid implants, biodegradable polymeric hydrogels don't need to be surgically removed after use [30]. An advantage with using temperature-responsive block copolymers that gels in water, as drug carriers, is the ability to make these preparations without using any organic solvents [18].

2.4.1 Gelation mechanism of BAB type polymers

The gelation of BAB polymer has been discussed by D.S. Lee et al. They researched the temperature-responsive PLGA-PEG-PLGA polymer, and developed a general theory for the gelation process of BAB polymers (as seen in Figure 12). Here they discussed that both the

hydrophilic PEG block (A-block) and the hydrophobic PLGA blocks (B-block) plays an important role in the sol-gel-sol transition. At low temperature the polymers self-assemble into micelles. With increasing temperature the PLGA blocks become even more hydrophobic. This increases the bridging and aggregation between the micelles. Above a certain temperature the hydrophobic core of the micelles shrink (because the hydrophobic block has a LCST). At the same time the PEG block (which is the outer shell of the micelles) will become dehydrated. The hydrogen bonds brake with increasing temperature. These factors combined causes the micelles to undergo a phase separation [31]. It should also be considered if the gradually dehydration of the PEG block promotes connection of micelles under gelation. When the surfaces of the micelles become more hydrophobic we get increased hydrophobic interaction between micelles and more connection points in a gel network.

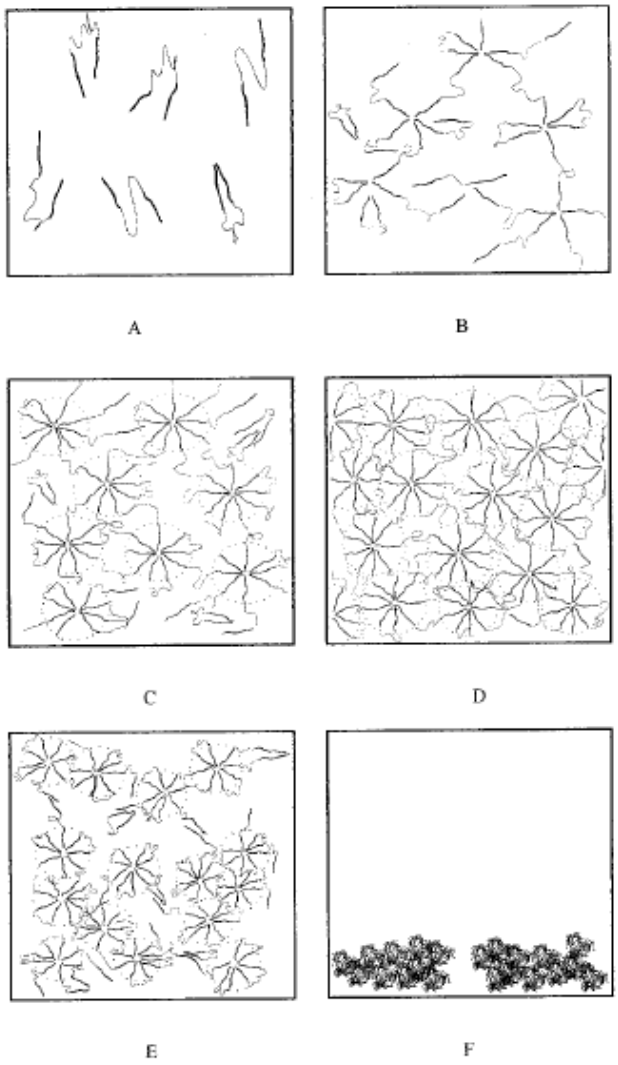

Figure 12. The possible micellar gelation process for BAB-type triblock copolymers in water. The figure is collected from an article by D.S. Lee et al. [31].

2.5 The Hofmeister effect on polymers

Franz Hofmeister first observed that the aptitude of salts to precipitate certain proteins from aqueous solution follows a recurring trend [32, 33]. This has been named the Hofmeister series, and a typical order of the anion series is shown below:

$$CO_3^{2-} > SO_4^{2-} > S_2O_3^{2-} > H_3PO_4^{-} > F^{-} > Cl^{-} > Br^{-} \approx NO_3^{-}$$
$$> ClO_3^{-} > I^{-} > ClO_4^{-} > SCN^{-}$$

The ions on the left side are called kosmotropes. They are considered as the "water making structures" because of their thick hydration shell. The group consists of small ions with high charge density. When these anions are present in an aqueous solution of polymer we frequently observe an increase in surface tension, lower solubility of the polymers and aggregation of molecules (salting-out effects).

The anions on the right hand side of the series are referred to as chaotropes. Here we find large ions, with small charge density and high polarizability. This group of ions is considered as "water breaking structures" and has a thin hydration layer. When these anions are added to aqueous solutions of polymers we observe the opposite effect than for adding kosmotropes. The solubility increases, and we observe a salting-in [33, 34].

2.6 Polymer characterisation:

There are a lot of different methods that can be used to characterise the properties of polymer systems. Combining the results from measurements of the microscopically gel properties for a polymeric hydrogel, and the chain interactions on the nano level, will give us a full impression of the system. The following sections under 2.6 will give an overview of different well used methods in investigating polymeric systems.

2.6.1 Cloud Point determination

Turbidity measurements can be used to characterise phase transitions in polymer samples. The critical temperature that gives a microscopic phase separation is named the cloud point (CP). We can determine CP via this method. We can calculate the turbidity from the signal from an instrument that utilizes a scanning diffusive light scattering technique (Figure 13). This method has both high accuracy and high sensitivity. A light beam is focused on the sample. The scattering intensity signal of the sample is monitored by an optical system with a matrix of light scattering detectors, which is situated above the sample [35]. The relationship between the signal and the turbidity is determined to be:

$$\tau = 9.0 * \ 10^{-9} * S^{3.751} \qquad (2)$$

Were τ is the turbidity and S is the signal.

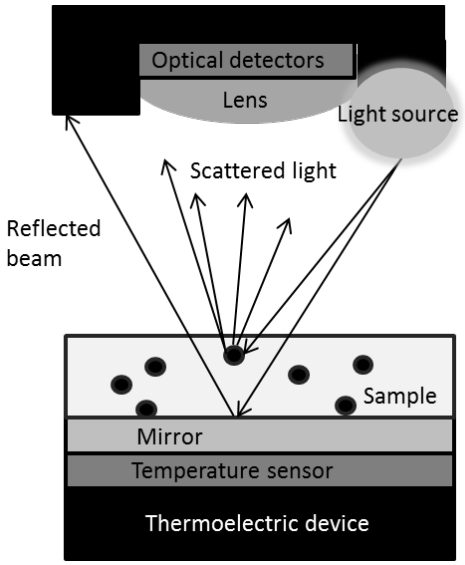

Figure 13. Schematic illustration of a cloud point analyser.

2.6.2 Rheology

The first definition of Rheology, wich is *the study of the deformation and flow of matter*, was accepted when the first American Society of Rheology was founded in 1929. In the beginning they focused on studying the properties and behaviours of materials like paint, lubricant, asphalt, rubber and plastic. Today there are scientiest working with rheology all over the world with widespread bakgrounds, including mathematics, physical chemistry, physics, pharmacy and engineering [36]. The application of rheology is growing.

Rheological measurements tell you something about how hard or soft a material is and indicates how fluid-like or solid-like it is. These characteristics are time dependent, meaning that we can see a change in the gel structure over a relatively short time range [37].

Viscoelasticity:

Polymeric fluids often show viscoelastic properties. The term 'viscoelastic' means the simultaneous existence of elastic and viscous properties in a material [38]. Viscoelastic materials tend to show a viscous response to slowly changing force, and an elastic behaviour when exposed to a force that varies quickly [39]. To explore the viscoelastic behaviour of a material one can impose small-amplitude oscillatory shearing, with the use of a rheometer with, e.g., cone-plate geometry. With a small enough strain amplitude (γ_0) the stress measured is controlled solely by the rates of spontaneous rearrangements or relaxation present in the fluid.

This is within the linear viscoelastic regime, were the shear stress (σ (t)) produced is proportional to the amplitude of the applied strain (γ_0) and its sinusoidally varying in time.[37] This can be expressed mathematically as:

$$\sigma(t) = \gamma_0 \left[G'(\omega)\sin(\omega t) + G''(\omega)\cos(\omega t)\right] \qquad (3)$$

Were ω is the frequency of oscillation in units of radians per second. The term proportional to $G'(\omega)$ is in phase with the strain and is often called the storage modulus. The term containing $G''(\omega)$ is called the loss modulus and is in phase with the rate of strain ($\dot{\gamma}$) [37]. In oscillatory shear experiments shear strain rate is a sinusoidal function of time expressed in this way:

$$\dot{\gamma}(t) = \frac{\Omega}{\tan\alpha} = \frac{\Omega_0 \cos(\omega t)}{\tan\alpha} \quad (4)$$

Here Ω is the steady angular rotation speed of the cone, and α is the cone angle.

The shear strain (γ) is the time integral of the shear rate [37]:

$$\gamma(t) = \frac{(\Omega_0/\omega)\sin(\omega t)}{\tan\alpha} \quad (5)$$

Rheology measurements:

There are different methods that can be used to determine viscoelastic behaviour. For measuring rheology it is useful to use a rheometer. The rheometer measures rheological properties of a complex fluid as a function of deformation. You can equip the rheometer with several different geometries, for examples a cone-plate, a cylinder or a plate-plate [37] as shown in Figure 14.

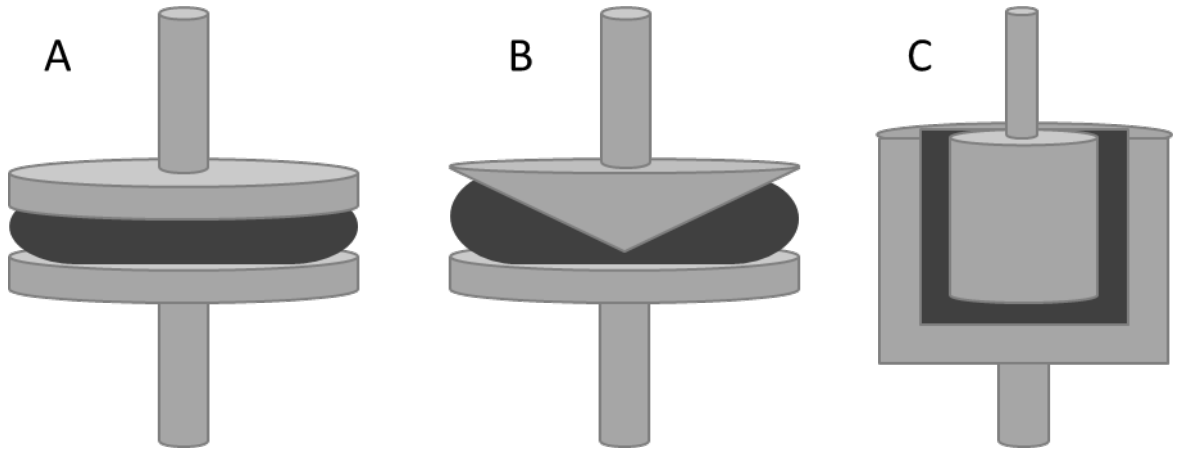

Figure 14. A) Plate-plate geometry. B) Cone-plate geometry. C) Cylinder.

Oscillatory shear measurements:

One of the most used dynamic methods is oscillatory shear measurements. With this test one can cover a wide frequency range, which is important if the material has a broad spectrum of relaxation times [36]. By using the cone-plate geometry one can achieve this kind of deformation by rotating the cone with an angular velocity that oscillates sinusoidally. The

strain amplitude has to be small to stay in the viscoelastic regime; you can explore the limit for a specific polymer system by doing an amplitude sweep.

Gel point:

As found by Winter and Chambon in 1986, the polymer system exhibits power –law relaxation behaviour at the gel point [40-42]. The loss tangent tan δ *(=G''/G')* is independent of frequency [43]. This can be seen by plotting the tan δ against time or temperature at different frequencies. At the gel point the curves for different frequencies will cross as see in Figure 15. One can therefor use a small amplitude frequency sweep to determine the gel point for a viscoelastic sample.

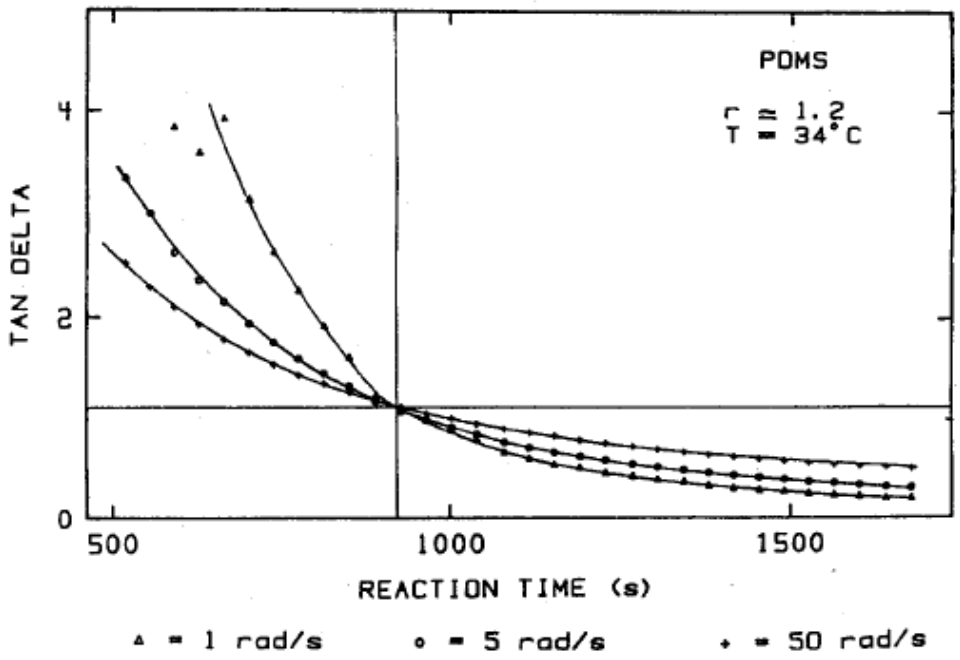

Figure 15.The tan delta for tree different frequencies in a small amplitude oscillatory shear experiment. The sample is a crosslinked poly(dimethylsiloxane) (PDMS) system. At the gel point the curves pass through a single point and tan delta is independent of frequency. The figure is collected from a paper by E. Holly et al. [43].

Because of the power law behaviour, a log-log plot of G' and G'' against angular frequency will show linearity at the gel point. The two curves will be parallel. This can be tested in another way by plotting the slope of G' and G'' curves at different times or frequency (depending on what we want to detect). The n' and the n'' curves will crossover where the slope of G' and G'' is equal (they are parallel). The value of n at the crossover is the relaxation exponent. This method is another way to detect a critical gel point [37].

Gel strength:

The gel strength parameter (S) can be used to describe the stiffness of the gel network. S can be expressed by the following equation:

$$G'(\omega) = \frac{G''(\omega)}{\tan(\frac{n\pi}{2})} = \Gamma(1-n)\cos\left(\frac{n\pi}{2}\right) S\omega^n \quad (6)$$

Where Γ( ) is the gamma function. n is the relaxation exponent and for n < 0,5 the G' > G'' while for n > 0,5 the G' < G'' [37], and tan(nπ/2) equals tan(δ) [44]. This equation is mainly used to determine the gel strength at the gel point for chemically crosslinked gel networks, but we can also use the principle to look at the gel strength for physical gels. The gel strength is dependent on the cross-linking density and molecular chain flexibility expressed via the relaxation exponent.

The relaxation exponent (n) varies for chemical gel from 0.19-0.92, and can be even lower for physical gels. It has been proven that increasing entanglement along the polymer chains in physical gels gives a lower value of n [37]. A low n value is equal to higher gel strength as seen in equation 6.

We can both have strong and weak physical gels. This is dependent on preparation conditions, which polymer that has been used, what kind of bonds that are formed and concentration of polymer. A strong physical gel is like a soft-solid (corresponding to a covalently bond chemical gel) whilst a weak physical gel is closer to a viscoelastic liquid [45].

2.6.3 Small Angle neutron scattering (SANS)

In the beginning of the seventies scientists started using neutron scattering in the field of polymer science in Grenoble. This has later spred to many other laboratories world wide [46].

The SANS technique is based on a beam of neutrons sent through the sample you want to investigate (Figure 16). The scattering pattern will give you information about structure of the sample. For doing SANS tests, especially on dilute samples, you need contrast. By using deuterium oxide (D_2O) you reduce incoherent scattering that adds to the background scattering. Using D_2O instead of H_2O increases the scattering contrast between the solvent and copolymer [47].

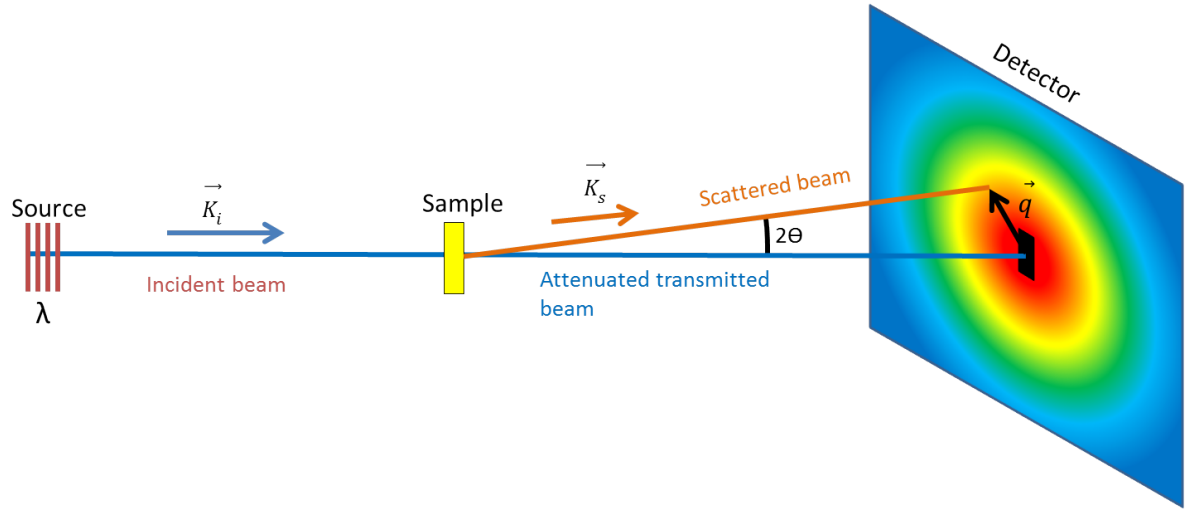

Figure 16. An overview of a SANS instrument.

The scattering vector, as shown in Figure 16, is given by:

$$\vec{Q} = \vec{k_s} - \vec{k_i} \tag{7}$$

Here $\vec{k_s}$ is the initial wavevector and $\vec{k_i}$ the final wavevector [47]. If the scattering process is completely elastic the modulus of Q can simply be expressed by the following equation:

$$Q = 4\pi \frac{\sin(\theta)}{\lambda} \tag{8}$$

Where θ is half of the scattering angle, and λ is the wavelength [48].

If the incident wavelenght is fixed, as it usally is in reactor spectrometers, the Q is directly related to the scattering angle. With the use of spectometers on pulsed source, however, you may use fixed angles and variable incident wavelenght to scan Q [46]. An illustration of the scattering from a wide Q range is given in Figure 17.

$$\frac{2\pi}{Q} = d \tag{9}$$

Here d is the distance probed in the sample. This equation shows the inverse releationship between Q and the distance. From this we can state that scattering at small angles probes large length scales.

The number of neutrons observed ($I(Q)$) by the detector is given by the following equation:

$$I(Q) = f(\sigma) \times C(Q) \times S(Q) \quad (10)$$

Here *f(σ)* represents the neutron-nucelear interaction as a fuction of the scattering cross section (*σ*), *C(Q)* represents all the influetial factors caused by the spectometer design (detector size, incident flux etc.) , and *S(Q)* is a structure factor that can be converted back to the spatial arrangments of the scattering nuclei [46].

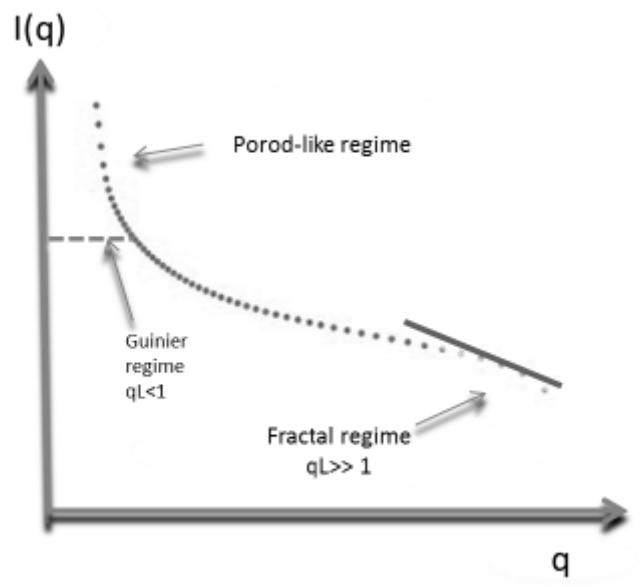

Figure 17. The SANS scattering over an extended q range. Illustration is collected from the thesis of N.K. Khorshid [49].

The shape of self-assembled BAB type polymers in solution predicted by SANS data:

To obtain more detailed information about the structure of micelles from SANS data we need to model the results. The structures of the self-assembling micelles depend on the packing parameter as described in section 2.3. The structure of a BAB type polymer with a sufficient long hydrophilic B block is predicted to form flower-like spherical core shell micelles in solution. However, with decreasing hydrophilic A block, the effective area of the hydrophilic "head" group is decreased. According to equation 1 the packing parameter will then increase. We can therefor suspect that these polymers will form elongated structures (cylinders). We therefore have to use different models to explain the structure of micelles depending on the length of the hydrophilic B block in an ABA –type polymer.

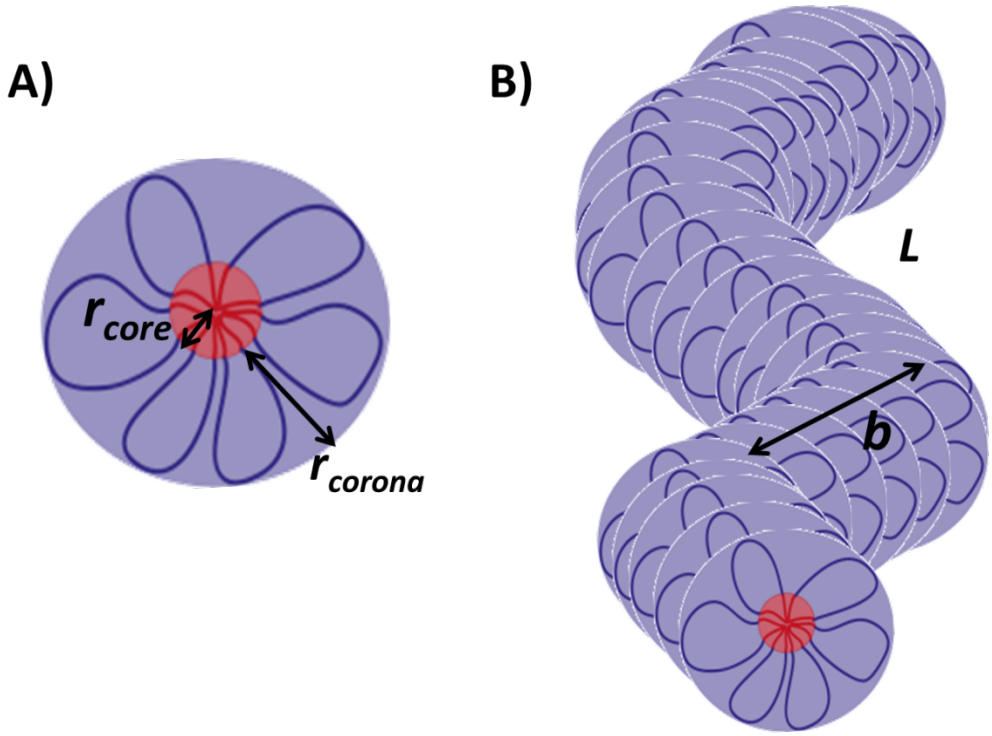

Figure 18A) spherical flower-like micelle of a BAB type polymer. R_{core} is the radius of the core while R_{corona} is the shell thickness. B) worm-like micelle. b is the Kuhn length and L is the average length of the micelle.

The model used to describe spherical core shell structures (Figure 18A) can be given by this general expression:

$$I(Q) = \left(\frac{N}{V}\right)(\Delta SLD)^2 Vp^2 P(Q) \tag{11}$$

where *(N/V)* is the number density of particles, *ΔSLD* is the difference in scattering length density of the polymer compared to the solvent, *Vp* is the volume of the particles and *P(Q)* is the form factor. The model is described in detail in Appendix A.

The probable structure of BAB type polymers with a shorter B block is cylinders; the cylinders can be characterised as worm-like if the cylindrical chains are flexible (Figure 18B). In these micelles the water soluble A block acts as a corona around a core consisting of the hydrophobic B blocks. The core consists of polymer (mainly B block) and no water. The shell consists of extended polymer chains and some amounts of solvent.

The scattering intensity as a function of the scattering vector can be described by the following expression [50]:

$$I(Q) = \frac{N_{polymer}}{V * p_{worm}} * P_{cs-worm}(Q) \quad (12)$$

where $N_{polymer}/V$ is the number density of polymer molecules, p_{worm} is the aggregation number for the wormlike micelles. $P_{cs\text{-}worm}(Q)$ is the formfactor for the wormlike micelles (described in detail in appendix B).

3 Materials and Equipment

3.1 Chemicals

Milli-Q Ultrapure (type I) water	Merck Millipore, Oslo, Norway
0.01M Phosphate buffered saline – powder pH 7.4 (MFCD00131855)	Sigma- Aldrich, Steinheim Germany
Deuterium oxide	The Institute of Energy Technology, Kjeller, Norway

3.2 Polymer

To find a suitable polymer matrix we screened several different polymers, all consisting of a hydrophilic PEG spacer and at least one PCL block. As a result of these tests we ended up with two polymers that showed promising properties.

The two polymers that have been investigated are amphiphilic triblock copolymers consisting of a hydrophilic PEG block in the middle and two hydrophobic blocks at each end. The hydrophobic block consists of randomly copolymerised LA and CL groups as seen from the structural formula in Figure 19.

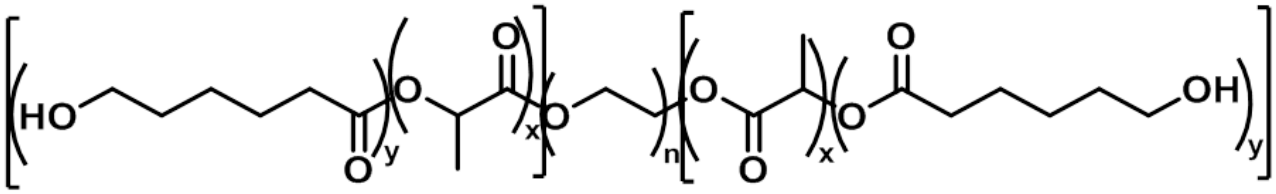

Figure 19. The structures of the polymers were: y = number of Caprolactone units, x = number of lactic acid units and n = number of polyethylene glycol units.

In Table 3 the ratio between the different monomers in the polymers and their molecular weights are presented (both reported from NMR and GPC measurements). The two polymers have approximately the same hydrophobic blocks whilst the hydrophilic group varies. The PCLA-PEG(1500)-PCLA polymer has a slightly higher polydispersity index than PCLA-PEG(1000)-PCLA.

Table 3. The chemical composition and molecular weight for the two polymers that are analysed in this master project.

Sample	**Block length**	**Mw PEG***	**Mn (NMR)**	**Mw/ Mn (GPC)**	**PDI**
PEG(1000)	(CL/LA)5/4-(EG)23-(CL/LA)5/4	1000	3280 (1140-1000-1140)	4210/ 3300	1.28
PEG(1500)	(CL/LA)5,5/3,9-(EG)34-(CL/LA)5,5/3,9	1500	3860 (1180-1000-1180)	5430/ 4090	1.32

*Mw for PEG as reported by the manufacturer.

Both polymers have been synthesised by Dr. Kaizheng Zhu at the Department of Chemistry at the University of Oslo.

3.3 Equipment

Balance:

Sartorius Extend ED224S	Sartorius, Göttingen, Germany

Automatic Pipettes:

Finnpipette, U27916 200-1000µL	Thermo Electron , USA
Finnpipette, V68945 1-5ml	Thermo Electron , USA

Mixer:

Vortex Genius 3	IKA Works GmbH and Co, Staufen, Germany

Water bath:

Refrigerated Circulators model ED	Julabo Labortechnik GmbH, Seelbach, Germany

Rheology:

Physica MCR 501 rheometer	Anton Paar GmbH, Germany
Physica MCR 301 rheometer	Anton Paar GmbH, Germany
CP75-1 cone, part number 79042	Anton Paar GmbH, Germany
CP25-4 cone, part number 303420	Anton Paar GmbH, Germany

Turbidity:

NK60-CPA cloud point analyzer	Phase Technology, Richmond, BC, Canada

SANS:

Small angle neutron scattering apparatus	Institute for Energy Technology, Kjeller, Norway

4 Experiments

4.1 Sample preparation

All solutions were prepared by weighing the polymer, based on desired concentration, in an appropriately sized sample glass. The polymer was then dissolved in a weighed amount of solvent (depending on the experiment). The sample was heated to 50 degrees in a heating cabinet for 5 minutes, and then stirred on a vortex mixer for 1 minute. The sample was heated to break down the crystalline structure and thus speeding up the dissolution process. Further, the sample was kept in the refrigerator until the polymer was fully dissolved. The time of this depended on type of polymer and concentration, but 48 hours was sufficient in most cases.

For the SANS measurements the solutions were prepared in deuterium oxide (D_2O). This solvent was used instead of H_2O to reduce background scattering.

For the rheology measurements both Mili-q water and phosphate buffer of pH 7.4 was used.

4.2 Tube-inverting method

Aqueous solutions of the polymers were prepared in various concentrations. The concentrations tested were 10, 15, 20 and 30 weight percent for both polymers. 1 ml of each solution was prepared in glass tubes. The tubes were kept in a water bath and heated up from 5 to 45°C. The sample was kept at this temperature for 10 minutes before inspection, to ensure equilibrium in the system. The samples were inspected at every degree. The sol-gel transition temperature was determined by flow to no-flow criterion over 1 minute.

4.3 Turbidity measurements

The turbidity was measured with an NK60-CPA cloud point analyser (Figure 20) in the temperature range 10-60 °C. 0.15 mL of the sample was placed with a micropipette onto a special glass plate that is covered with a thin metallic layer of high reflectivity (a mirror). The sample surface is covered with 0.15 mL of highly transparent silicon oil to prevent evaporation of the sample at elevated temperatures. The apparatus is equipped with a Peltier plate that is responsible for adjustment of temperature. The temperature was increased at a rate of 0.2°C/min. All the samples were heated and cooled two times. Only the second heating was used in the analysis of the results. The sample was soaked for 150 seconds at the lowest and highest temperature for equilibrium. The measurements were performed two times for every sample; the results have shown to be reproducible. The turbidity was calculated by using equation 2. The CP was obtained by a plot of turbidity as a function of temperature.

The concentrations tested were 1 and 20 weight percent for both polymers.

Figure 20. Picture of the NK60 cloud point analyser.

4.4 The rheology measurements

The rheology measurements were performed using an Anton Paar-Physica MCR 501 and MCR301 rheometer (seen in Figure 21). The rheometer was equipped with cone-plate geometry. In the experiments two different cones were used: CP75-1 with a diameter of 74.979 mm and an angle of 0.984°, and CP25-4 with a diameter of 24.980 and an angle of 3.995°. The smaller cone was used for samples with high concentrations to reduce the required amount (a difference in results caused by using different cones was checked and eliminated). The instrument has a temperature element (Peltier element) which gives an effective control of the temperature (±0.05 °C) over the whole temperature range used in the experiments.

To prevent evaporation a thin string of silicon oil was applied (the layer of oil does not affect the viscoelastic response of the sample). The rheometer has been calibrated with water and standard high viscous oil before performing any experiments.

An amplitude sweep was preformed to estimate the yield value. The appropriate amplitude for further measurements was chosen to ensure that they were conducted in the linear viscoelastic region. In the amplitude sweep the frequency was held constant at 1Hz, while the strain (γ) was increased from 1 % to 100 %, and then reversed.

The frequency sweeps were all preformed using the same settings except for an increase in time between each measurement point when using the smaller cone to reduce noise. The amplitude was held constant at 1 %, and the frequency was varied between 0.01-100Hz. There were measured tree loops of this frequency sweep at each temperature, with a 60sec brake in-between each loop (this had been investigated to be sufficient to recover the structures). An average of these three loops was used in the analysis of the results. The measurements were performed at every degree from 5 to 45°C. The sample was held at each temperature for 20 min before performing the measurements to ensure equilibrium in the sample.

The concentrations tested were 10, 20 and 30 weight percent for both polymers. To check for reproducibility the measurement of 20 wt% of PCLA-PEG(1000)-PCLA was repeated three times with fresh samples. This was used as a statistical centre point. The amount of available polymer is limited so I was not able to repeat every measurement three times.

The gel point was determined by using the method that was developed by Winter and Chambon and the crossover between n' and n'' (as described in section 2.6.2).

Figure 21. A picture of the Anton Paar Physica MCR301 instrument.

4.5 Small angle neutron scattering measurements

All the SANS experiments were carried out at Institute for Energy Technology (IFE, Kjeller) as seen in Figure 22. The SANS instrument obtaines neutrons from the reasearch reactor Jeep-II. Two different detector distance (1.0/3.4 m) and to different wavelengths (5.1/10.2 Å) were employed in order to obtain the largest possible Q-range.

For the PCLA-PEG(1000)-PCLA polymer we measured samples at five different consentrations: 1, 10, 15, 20 and 30 weight percent. The PCLA-PEG(1500)-PCLA polymer was measured at 1 and 20 weight percent. The solutions were filled in 2 mm Hellma quartz cuvettes.

The samples were measured at different temperatures from 10°C to 49°C. After heating to 49°C the samples were cooled and kept for a few houres first at 20°C and then lastly at 10°C.

Standard reduction of the scattering data was preformed after finishing the experiments. Here the transmission was measured separately, and absolute scattering cross section (cm-1) was calculated by taking into account the contribution from empty cell and general background.

After the data reduction, fitting of the scattering curves was prefomed in Qtikws. In the prelimenary analysis of the SANS data, a core-shell spherical model was fitted to the 1 wt% sample of PCLA-PEG(1500)-PCLA. The results from the PCLA-PEG(1000)-PCLA were initially tried to fit a clustered core-shell model, but later changed to a worm like cylinder model for a better fit. The density (and corresponding scattering length density) of the hydrophilic PEG block was altered with temperature as described by C. Sommer et al. [51].

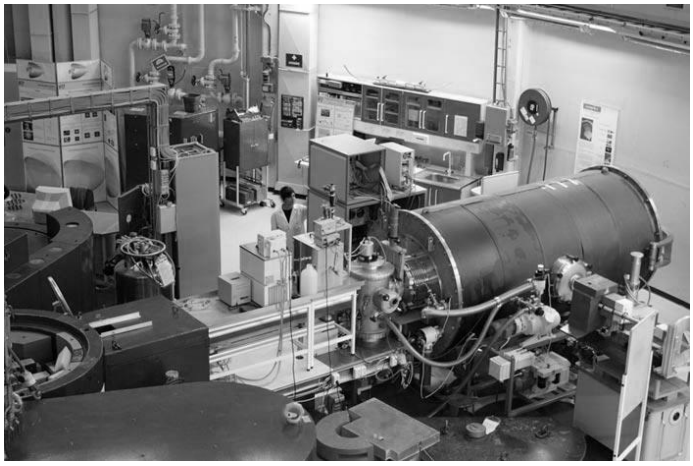

Figure 22. Picture of the SANS installation at IFE, Kjeller.

5 Results and Discussion

5.1 Phase diagram

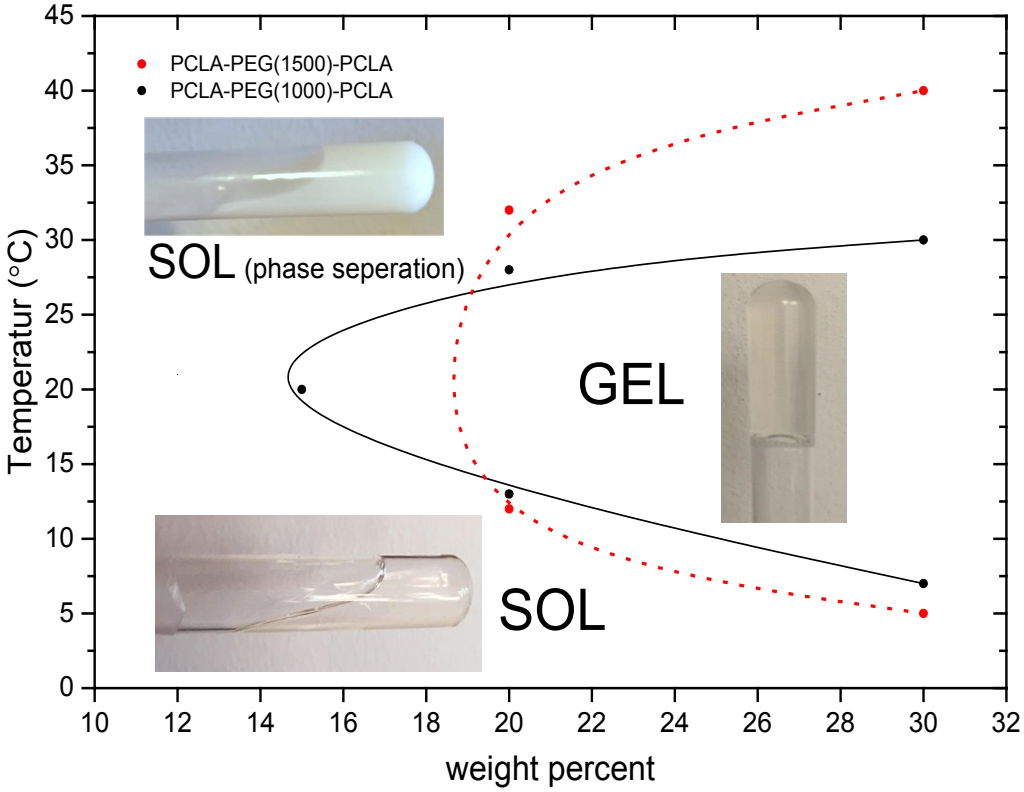

Figure 23. Phase-diagram for the two polymers: PCLA-PEG(1000)-PCLA (-----) and PCLA-PEG(1500)-PCLA (- - -). The line is added to guide the eye between the measured points. The pictures is featuring a 20 wt% sample of the PCLA-PEG(1000)-PCLA polymer showing the sol phase, gel phase and lastly the phase separation.

Through conducting a tube inverting experiment with both polymers, the phase diagram as shown in Figure 23 was obtained. The polymers exhibits three physical states: sol phase with free micelles, hydrogel phase with an interconnected network, and precipitation at the higher temperature range. In the gelling samples the phase separation is observed first as the transition from a clear gel to a "white gel". Then as the temperature increases the gel network starts to melt, and eventually precipitation of the sample.

From the tube tilting experiment it was indicated that a higher concentration of the PCLA-PEG(1500)-PCLA is required to form a gel network, than of PCLA-PEG(1000)-PCLA. The gel phase for the polymer with the longer PEG spacer has a wider temperature range. The observations from doing this experiment needs to be investigated further by other methods to obtain a full picture of the polymer systems.

5.2 Cloud point changing with length of the PEG spacer

To investigate the phase separation, which was observed in the tube tilting experiments, turbidity measurements were performed. We can obtain a cloud point (CP) for the two polymers at different concentrations, from the results. In Figure 24 it is shown that the CP is shifted drastically to higher temperatures when the length of the hydrophilic PEG block is increased. For the polymer with the shorter PEG spacer a CP of 38 °C for 1 wt% and 23 °C for the 20 wt% sample is obtained. The highest turbidity we observe increases with concentration.

For PCLA-PEG(1500)-PCLA a CP of 52°C for 1 wt% and 47°C for 20 wt% is found. Also here the peak turbidity increases with higher concentration.

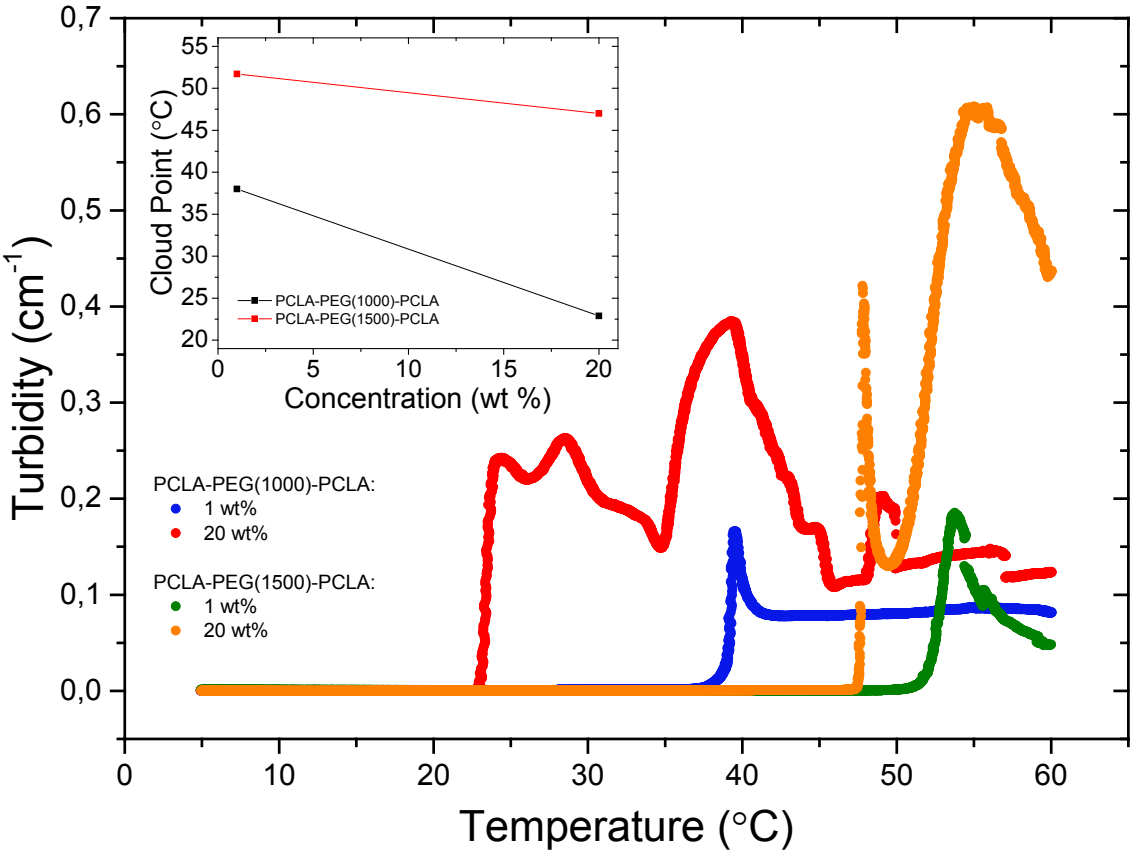

Figure 24. The turbidity of the PCLA-PEG(1000)-PCLA and PCLA-PEG(1500)-PCLA polymer at aqueous solutions of 1 and 20 wt% as a function of temperature. The inset graph shows the Cloud Point as a function of concentration for both polymers.

The dilute sample of both polymers shows a maximum turbidity followed by a decrease when the sample is heated further. This has also been observed by N.K. Khorshid for a very similar polymer system consisting of PLGA-PEG-PLGA [49].

The results for the 20 wt% sample of the PCLA-PEG(1000)-PCLA polymer is in agreement with the observations from the tube inverting test. We observed a phase separation at approximately the same temperature. For the other polymer the observation of increased turbidity and the results from the cloud point analysis is not fully coherent. Here the visual observation showed a transition from gel to sol at a lower temperature than the turbidity measurements indicate as a cloud point. This may indicate that this polymer system gel melts at a lower temperature than the phase separation. In the turbidimetry measurements the sample is heated at a higher rate than in the tube tilting experiments. This might lead to an overestimation of the cloud point.

The turbidity results prove that both concentration of polymer and length of PEG spacer highly affect the CP (inset graph in Figure 24). The CP is observed at a higher temperature for PCLA-PEG(1500)-PCLA than for PCLA-PEG(1000)-PCLA, because the polymer with the longer PEG spacer is more water soluble. A similar trend was also identified for PLGA-PEG-PLGA in a study by N.K. Khorshid. She explained this tendency with a more pronounced enhancement of hydrophobicity at higher temperatures for polymers with a shorter hydrophilic block. An additional explanation was that N.K. Khorshid found the micelles for the polymer with the short PEG spacer to be less stable, and therefore more easily form aggregates [49]. We will investigate this further for our polymer system in the analysis of small angle neutron scattering data.

5.3 The viscoelastic properties of PCLA-PEG-PCLA

From the tube inverting method we obtained some information about the viscoelastic properties of the polymer systems. This can be quantified more accurately by doing rheology measurements. From a pharmaceutical drug delivery perspective we can obtain some important information from the rheology results. To determine if these polymers are suitable as *in situ* gelling implants, we focus on studying the gel point and gel strength for the polymer systems.

5.3.1 Gel point

With help of the tube inverting method we got an indication of the temperature dependent gelation of the polymer systems. By analysing the results from rheology measurements we should be able to determine a more accurate gel point. The gel point determination will give us an idea if the two polymers can be used for *in situ* gel formulations.

PCLA-PEG(1000)-PCLA:

We could observe a gel at 7°C with using the tub inverting method for the PCLA-PEG(1000)-PCLA with a concentration of 30 wt %. To validate this result we use the theory from Winter and Chambon, as explained in section 2.6.2, to determine a gel point of the sample. The results from this analysis are shown in Figure 25.

The tan (δ) plot show a gel point of about 7°C where the curves for the different frequencies go through the same point. In the inset graph A (Figure 25) we see a cross over between n' and n'' at approximately the same temperature. I the inset graph B) (Figure 25) we see that G' and G'' is showing a linear trend. The curves for the two moduli are approximately parallel at the gel point. A gel point at ca 7°C is in agreement with the physical observations of the system as shown in the phase diagram for the polymer (Figure 23).

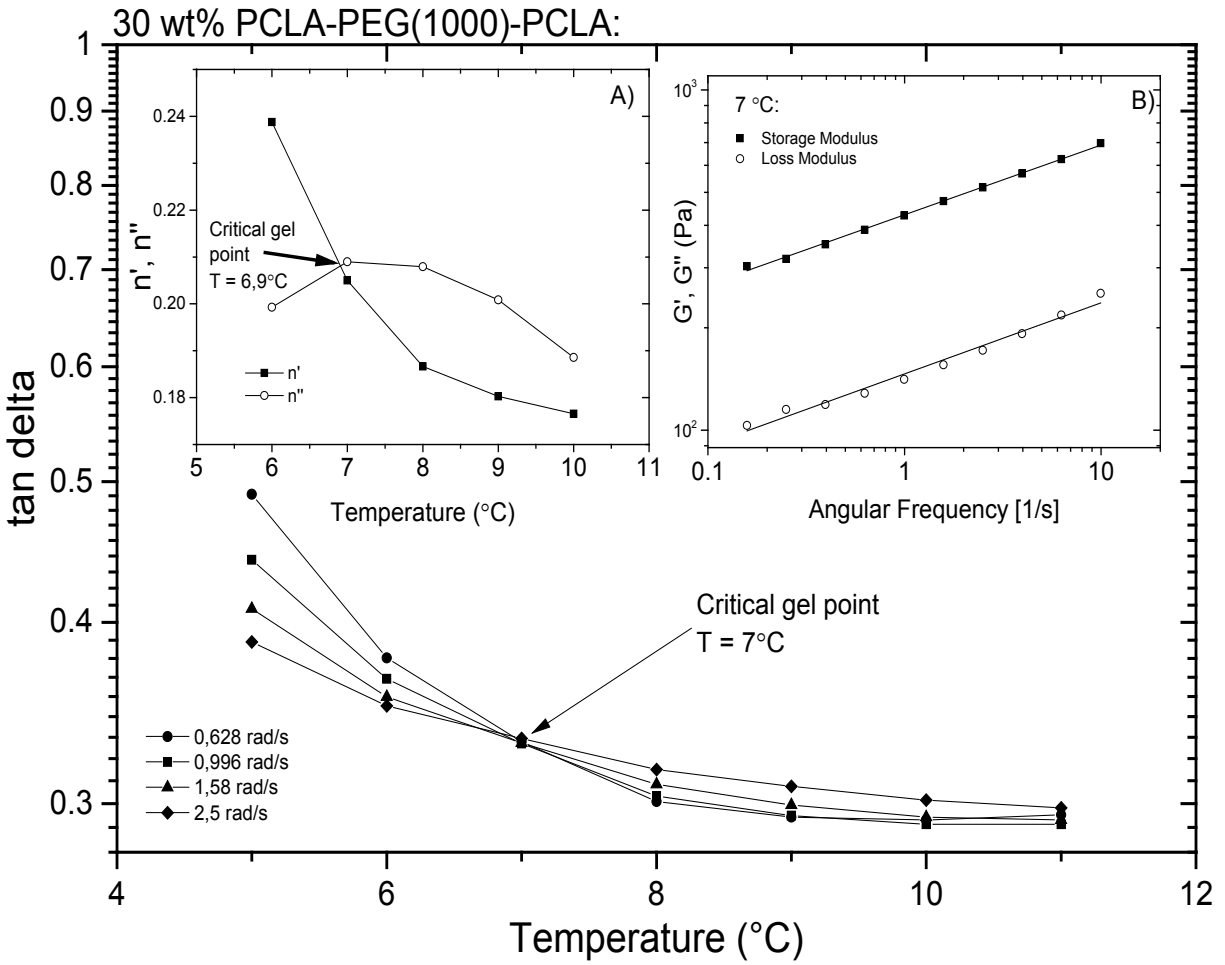

Figure 25. Tan(δ) versus temperature for the PCLA-PEG(1000)-PCLA polymer at 30 wt%. Inset graph A) shows the n' and n'' plotted against the temperature with an intersect at 6.9°C. Insert graph B) shows the G' and G'' versus Angular Frequency at 7°C (the gel point).

For lower concentrations of this polymer we cannot detect the same clear gel point. For the 20 wt% we observe a gel-like system at around 15°C by the tube inverting method. In Figure 26 we can see an insinuation to a critical point between 13 and 14 °C when we plot tan(δ) versus temperature at different frequencies. Inset plot A) and B) in Figure 26 shows that the G' and G'' is semi parallel at both temperatures. The values for G' and G'' increases drastically from 13 to 14 °C. From inset plot C) were n' and n'' is plotted against temperature, we see an intersect between the two exponents, but the trend is not as clear as for the 30 wt% sample (inset graph A in Figure 25). We should also mention that n' is higher than n'', which is usually the other way around after a critical gel point. From these results we are not able to prove that the system, at this concentration, fulfils the criteria as a gel even though we have observed this.

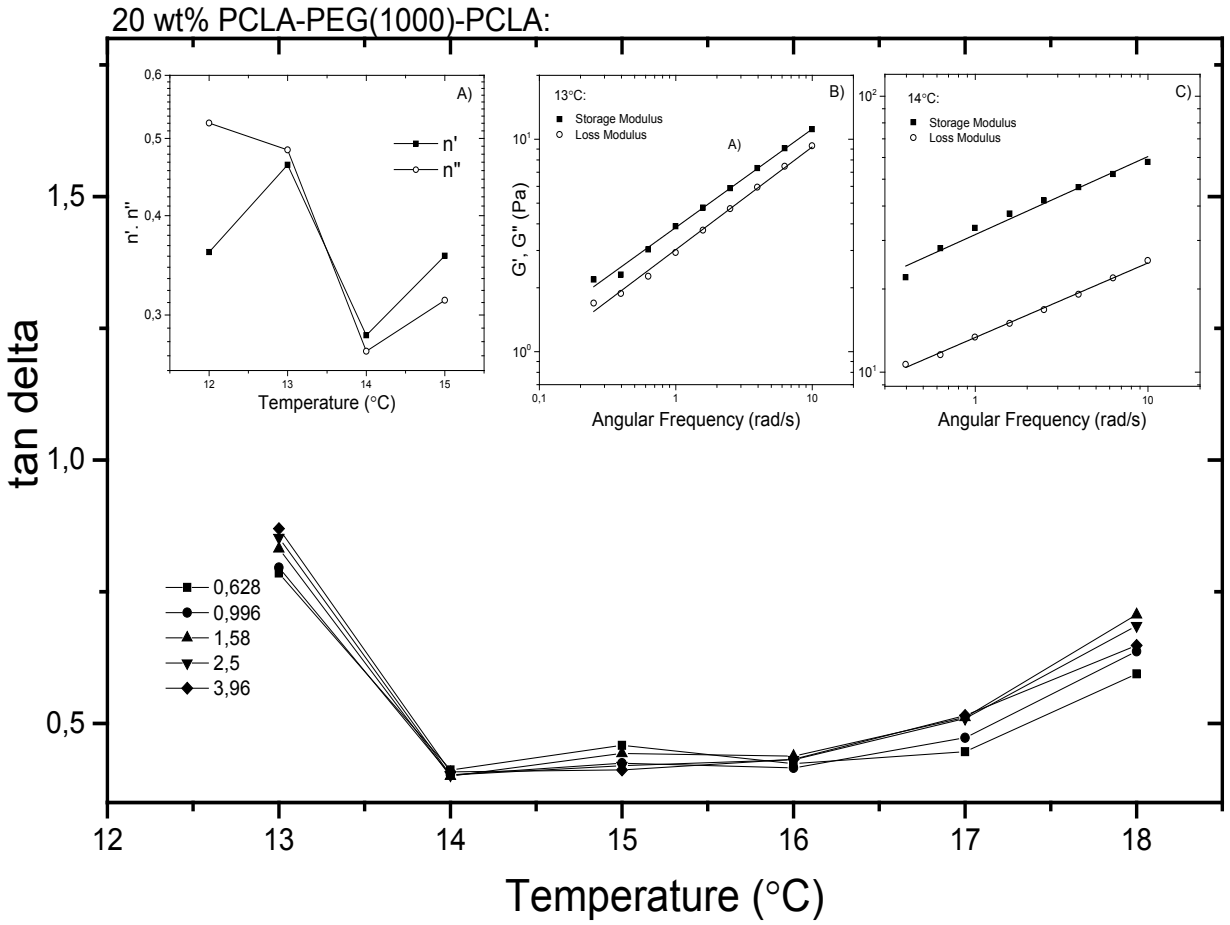

Figure 26. Tan(δ) versus temperature for the PCLA-PEG(1000)-PCLA polymer at 20 wt%. Insert graph A) shows the n' and n'' plotted against the temperature with a intersect at 13,5°C. B) shows the G' and G'' versus angular frequency at 13°C. Insert graph C) shows the G' and G'' versus angular frequency at 14°C.

The difference in the ability to determine a gel point between the higher concentration of 30 wt % and the slightly lower concentration of 20 wt % might be caused by the strength of the gel system. This will be elaborated further in section 5.3.2

PCLA-PEG(1500)-PCLA:

For the PCLA-PEG(1000)-PCLA we could determine a clear gel point at higher concentrations, while for PCLA-PEG(1500)-PCLA this has proven to be very difficult. The problem of determining GP has been reported in the literature for other gel systems like Pluronic by amongst others B. Nyström and H. Walderhaug [13]. In the case of Pluronic it is well established that the system forms a gel network at approximately 37°C. This has been identified by the tube tilting method. Even though we can observe a gel network it is not

possible to see the power law behaviour of a gel point. B. Nyström and H. Walderhaug were able to identify a crossover between G' and G'', the same as we observe at different frequencies. However as described by Winter and Chambon, this does not give an accurate estimate for a gel point [40-42]. In the paper by B. Nyström and H. Walderhaug they discussed that the reason for the unusual behaviour for Pluronic, points towards a very complex system with unusual properties [13].

In our system we observe some of the same behaviours as identified for Pluronic. We observe the sharp increase in dynamic viscosity with increasing temperature, and we see a gel system via the tube inverting method. However, we are not able to observe any frequency independence in a plot with tan (δ) as a function of temperature (Figure 27).

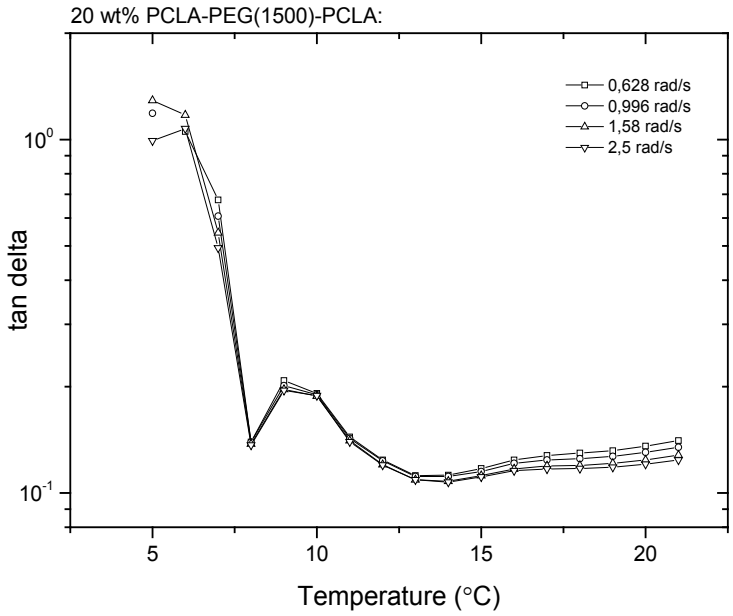

Figure 27. Tan delta as a function of temperature for 20 wt% of PCLA-PEG(1500)-PCLA in water at the frequencies indicated.

We can obtain some interesting information about our polymer system from Figure 27 even though we cannot determine a critical gel point from this graph. We see a drop in the tan (δ) value between 6 and 8°C, which might be associated with the growth of clusters of micelles, making G' measurable. The same tendency was seen for Pluronic [13]. By the tube inverting method we found a gel point of 12°C at this concentration. We see in Figure 27 that the tan(δ) has a small peak at 10°C and then decreases. Here the storage modulus is getting larger compared to the loss modulus, which indicates a more elastic behaviour. One possible

explanation for this could be that a network of interconnected micelles is formed at this temperature.

When plotting G' and G'' against temperature at different low frequencies, we see a crossover of the curves between 6 and 7°C (Figure 28). This gel point is at a lower temperature than indicated by the test tilting method. The same trend was found by B. Nyström and H. Walderhaug for the Pluronic system. Here they had an observed gel point of 37°C, but a crossover of G' and G'' at 34°C [13].

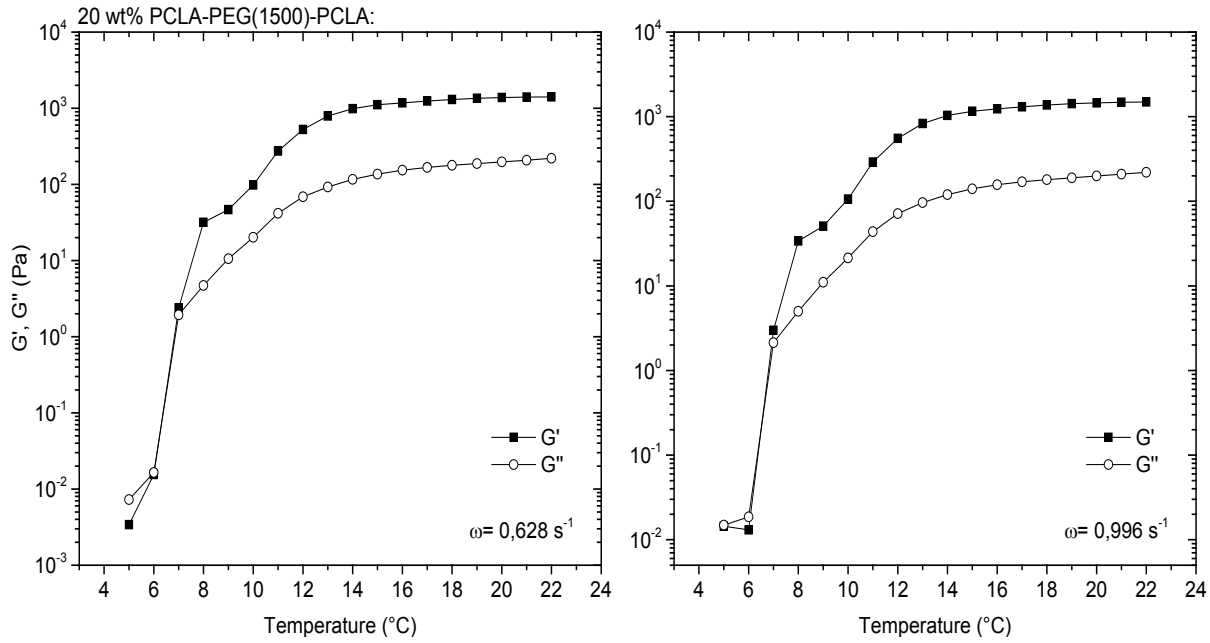

Figure 28. Temperature dependence of the storage modulus (G') and the loss modulus (G'') for the PCLA-PEG(1500)-PCLA (20wt%) at the frequencies indicated.

One possible explanation for this behaviour is that it is caused by the physical gel system having a gelation process that happens very gradually. We are therefore not able to determine a critical gel point. With increasing concentration and ultimately the number of micelles, the micelles begin to interact with each other and are forming bridges. When the concentration is high enough, all the micelles are connected in a network through these bridges resulting in a high viscosity.

Pharmaceutical application related to the gel point:

The gel points determined from the rheology measurements indicate that the polymer system form a gel at a temperature that is lower than we are aiming for. The idea that the drug formulation is to undergo gelation *in situ*, ideally requires a gel point that is slightly higher than room temperature. However, administering the drug at a lower temperature than room temperature (for example refrigerator temperature) might be an option. Injecting larger doses of cooled liquid into the patient might cause hypothermia. This will not constitute a risk for the patient if the acquired amount of drug that is injected is fairly small. However, even injecting small amounts of chilled liquids often feels uncomfortable for the patient and therefore influence the adherence. It might also be a problem that the drug formulation will form a gel in the syringe before being administered to the patient. Because of these issues we would like to adjust the gelation of the system to a higher temperature. Altering the chemical structure of the polymer might be an option for achieving this, for example changing the ratio between LA and CL, or the overall size of the polymer chains. This needs to be investigated further.

5.3.2 The degrees of entanglements in the polymer system and the resulting gel strength

We need to study the strength of the gel systems to determine if the system is suitable to act as an injectable implant for drug delivery purposes. In a physical gel system the degree of entanglements will give us an indication on how strong the gel network will be.

To be able to calculate the gel strength (equation 6) we need to be able to determine a critical gel point. We are therefore only able to calculate the gel strength for the 30 wt% sample of the PCLA-PEG(1000)-PCLA polymer. From this we find a gel strength of 364.8 $Pa*s^n$. We can compare this value for gel strength to a chemical cross-linked Poly(vinyl alcohol (PVA) that has been studied by A. L. Kjøniksen and B. Nyström. Because cross-linked gels are covalently bond networks we assume that these gel systems should have higher gel strength. In the study of PVA they found gel strengths ranging from just a couple of $Pa*s^n$ to ca. 600 $Pa*s^n$ depending on concentration of polymer and cross-linker [52]. We can therefore state that a 30 wt% sample of PCLA-PEG(1000)-PCLA has approximately the same gel strength as a 10 wt% sample of PVA with 22 mM glutaraldehyde (the cross-linking agent).

Because we are not able to give a quantitative answer to the gel strength for the rest of the samples, we need to look at alternative ways to obtain some information about the strength of the gel network. From the loss modulus we can calculate the dynamic viscosity of the polymer samples. Because we are working with a temperature responsive polymer we are interested in finding out how the dynamic viscosity evolves with increasing temperature.

For the polymer with the shortest PEG length (Figure 29A) we observe a clear temperature dependence. For the lowest concentration, of 10 wt%, we measure an increment from 0.02 Pa at 15 °C to 6.4 Pa at 20 °C. This is a 320 time increase of viscosity with only 5 degree increase in temperature, but the peak dynamic viscosity of 6.4 Pa is still low.

When we increase the concentration of polymer to 20 wt% the peak viscosity is at 28.5 ± 3.7 Pa which is 4.5 times higher than for 10 wt%. The rheology experiment for this concentration was repeated three times with fresh samples as a statistical centre point. The error bars are included in Figure 29A).

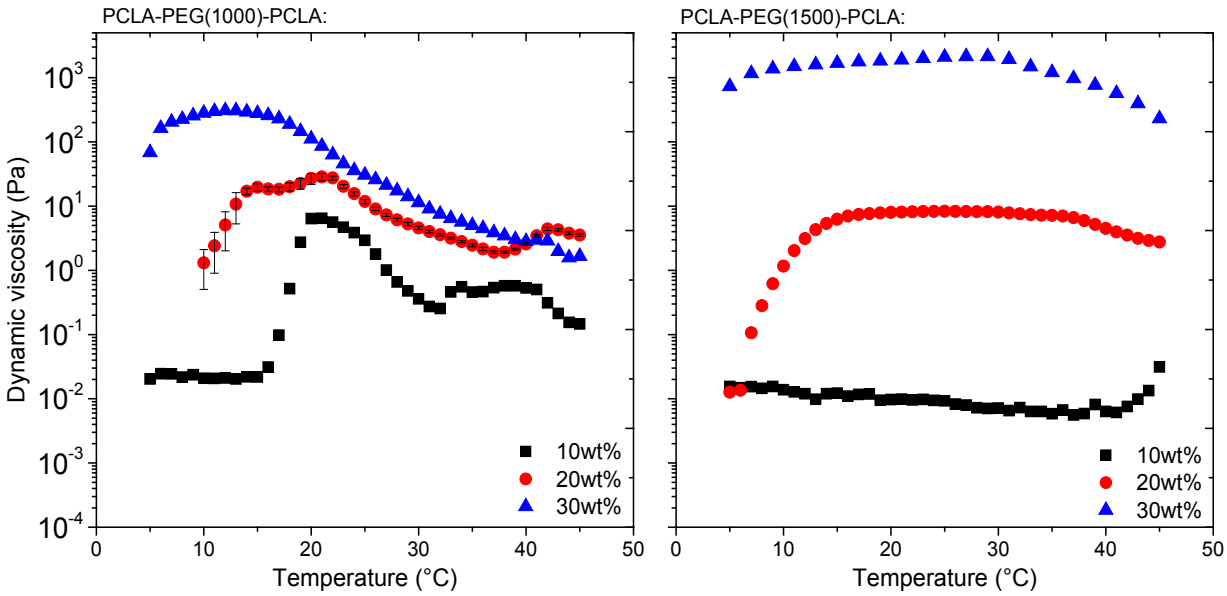

Figure 29. Polymer concentration dependence of the dynamic viscosity for the two polymers at a constant frequency of 0.1 Hz. A: PCLA-PEG(1000)-PCLA, B: PCLA-PEG(1500)-PCLA. Error bars for the 20 wt% system of PCLA-PEG(1000)-PCLA is the standard deviation of the mean viscosity after repeating the experiment three times.

When increasing the concentration of polymer, the increase in viscosity shifts to a lower temperature. This trend proceeds when we increase the concentration to 30 wt%. Here the dynamic viscosity is already at 68.5 Pa at 5 °C and increases to a peak of 307.32 Pa at 12 °C. From this we can conclude that the dynamic viscosity of this polymer is strongly concentration dependent, the peak value of 30 wt% is 48 times higher than for 10 wt%. The peak viscosity for the higher concentration is still quite low.

The difference in strength of the network might explain why we only were able to determine a gel point for the 30 wt% sample. At lower concentration the weak network might be disrupted even at the low frequencies that were used in the analysis of gel point. The definition of a gel network is not as clear for a physical gel as for a permanent chemically crosslinked gel. It is therefore open for discussion whether our system at low concentrations can be described as a gel. We observe that the 20 wt% polymer sample does not flow during 1 minute in the tube tilting method, but from rheology measurements we calculate a low dynamic viscosity, and are not able to determine a clear gel point.

In Figure 29B) we see the same graph for the polymer with the longer PEG block (PCLA-PEG(1500)-PCLA). At the lower concentration the dynamic viscosity is quite stable for about 0.005-0.015 Pa. When the concentration is increased to 20 wt% we observe a dramatic change. At this concentration the dynamic viscosity goes from 0.01 Pa at 5 °C to a stable

value of 8.2 Pa. This plateau reaches from approximately 14 to 37°C. When heating to higher temperature the viscosity decrease slightly. For the 30 wt% sample the viscosity is relatively high already at refrigerator temperature with a viscosity of 730 Pa at 5°C. At 27 °C the viscosity peaks at 2139 Pa, which is only a 2.93 time increase from the lowest temperature.

If we compare the results for PCLA-PEG(1000)-PCLA and PCLA-PEG(1500)-PCLA, we see that at 30 wt % we get a 7 times higher dynamic viscosity for the polymer with the longer PEG block. The viscosity of PCLA-PEG(1000)-PCLA undergoes larger changes with increasing temperature compared with the PCLA-PEG(1500)-PCLA polymer. The latter polymer can be described as being more stable upon heating. We need to investigate the structure of the polymer samples via small angle scattering to be able to explain why we observe a large difference in temperature dependence and overall strength of the network.

We can compare the dynamic viscosity for our system with other thermoreversible gel systems like for example Ethyl(hydroxyethyl)cellulose (EHEC), as studied by A. Kjøniksen et al in 1998. EHEC needs to be combined with an ionic surfactant to form a gel network, and in these experiments they have used the anionic surfactant sodium dodecyl sulphate (SDS). The EHEC-SDS system forms a gel at a relatively low concentration of polymer, but this depends on the amount of SDS. In these experiments the highest dynamic viscosity achieved is around 100 Pa (Figure 29) [53]. The dynamic viscosity for our system is higher at 30 wt% for both polymers, but at the lower concentrations it is significantly lower.

Another way to investigate the entanglements of the polymer samples is to analyse how the viscosity changes with increasing angular frequency at different temperatures, as plotted in Figure 30A) and B). For the PCLA-PEG(1000)-PCLA polymer (Figure 30A) we observe a significant frequency dependency at the lower temperature range. Here we see a clear trend that increasing frequency equals to lower η' values. This is typical for polymeric network systems that contain entangled or interconnected chains [13]. The curves for 35 and 45°C show no significant changes in dynamic viscosity over the frequency range. Here the PCLA-PEG(1000)-PCLA polymer displays rheological characteristics typical of untangled polymer solutions. These results are in agreement with the hypothesis of the gel system melting at higher temperature.

The PCLA-PEG(1500)-PCLA polymer (Figure 30B) shows some of the same tendencies as for the PCLA-PEG(1000)-PCLA at the lower temperature range. For higher temperatures we

observe a clear difference between the two polymers. For PCLA-PEG(1500)-PCLA the frequency dependence trend continues through the whole temperature range. This indicates that the polymer system has entanglements and interconnected chains even at 45°C. The slope of the curves is similar and we see that the value of η' increases with increasing temperature until it reaches an optimum at 25°C. At temperatures beyond 25°C, the dynamic viscosity decreases drastically even though we still have an interconnected network of polymer micelles.

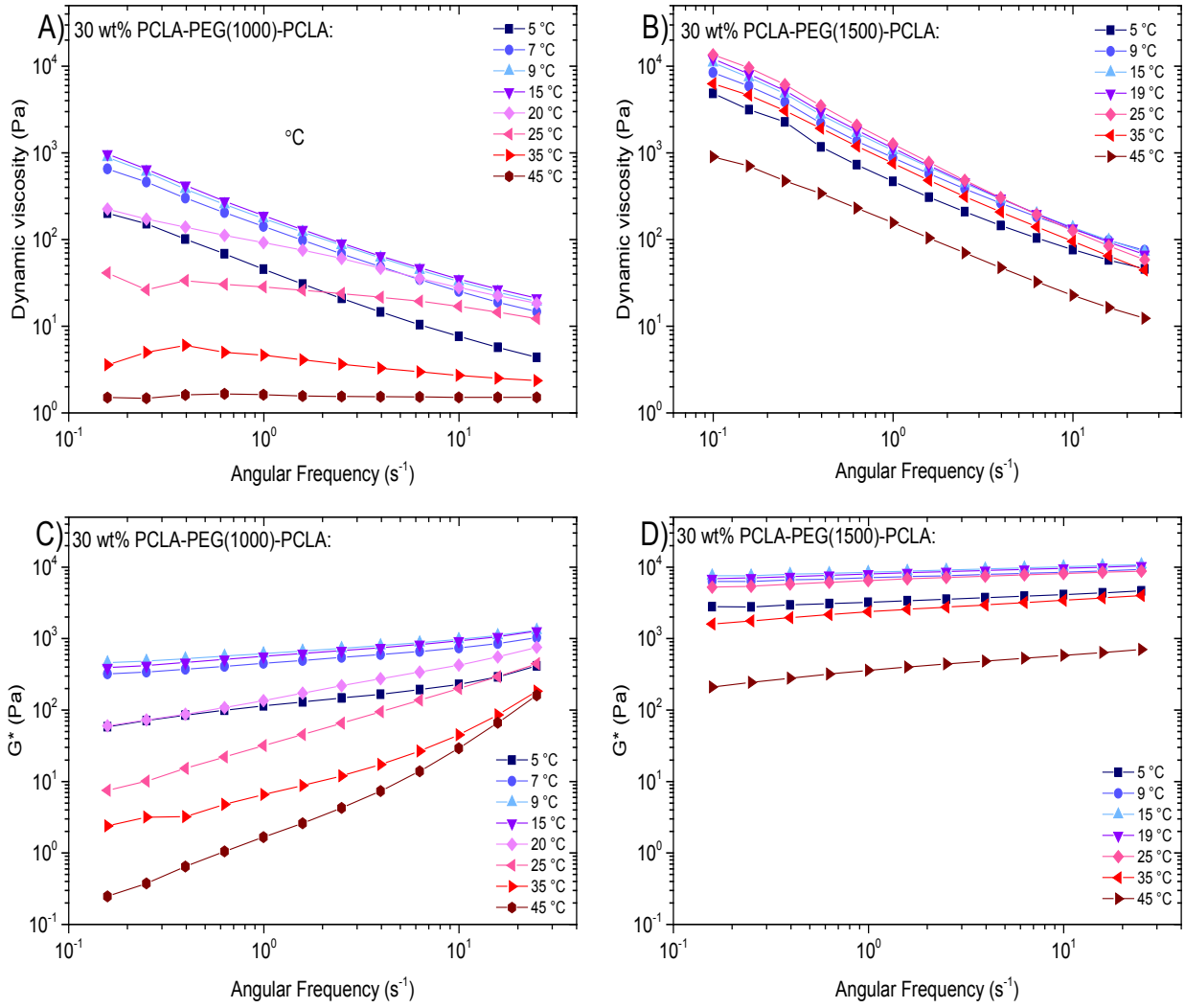

Figure 30. A) The dynamic viscosity as a function of angular frequency for 30 wt% PCLA-PEG(1000)-PCLA in water at indicated temperatures. B) The dynamic viscosity as a function of angular frequency for 30 wt% PCLA-PEG(1500)-PCLA in water at indicated temperatures. C) Frequency dependence of the complex modulus for 30 wt% PCLA-PEG(1000)-PCLA in water at the temperatures indicated. D) Frequency dependence of the complex modulus for 30 wt% PCLA-PEG(1500)-PCLA in water at the temperatures indicated.

In a viscoelastic system we have a combination of solidlike and liquidelike behaviour. We can plot the complex modulus against frequency to investigate which of these properties that is more dominant. Figure 30C and D) show a double-logarithmic plot of the complex modulus as a function of frequency for the two polymers. For the PCLA-PEG(1000)-PCLA polymer we observe that a solidlike behaviour is indicated at the lower temperatures, seen as a weak frequency dependence of G*. This is especially visible for the curves from 7-15 °C. For the higher temperature (45°C) a power law $G^* \sim \omega^{1.0}$ is observed. This indicates that we have a system in a liquidlike state.

The PCLA-PEG(1500)-PCLA (Figure 30D) displays this weak frequency dependence of G* over the whole temperature range. This again indicates a solidlike behaviour from 5-45°C in good agreement with a wide gel-phase in the phase diagram for this polymer (Figure 23).

Pharmaceutical application related to the gel strength:

In order to use the polymer system as an injectable implant for drug delivery, the gel network needs to be relatively strong and tight. We have not determined were the drug formulation should be injected in the patient. If we for example imagine injecting the implant intramuscularly, the gel network would need to be very strong because of the large strain from the muscles that are contracting. Another option is injecting it in an interstitium; here weaker gels might be acceptable. From the rheology measurements we observe that the viscosity of the gels might be too low for using the polymers as the gel matrix. This issue needs to be addressed in further studies and development of the polymer as a drug carrier.

We also need to have a tight network that prohibits the diffusion of the drug containing microparticles. We want the microparticles to sustainably release the Naltrexone drug while being constrained in the network. We have seen from looking at the frequency dependence that the system exhibits solidlike behaviour with a high degree of entangled polymer chains. From this alone we cannot conclude if the network is tight enough for our purpose, but we can investigate this further via small angle scattering.

5.4 Structural changes for the PCLA-PEG-PCLA polymer with increasing temperature

SANS measurements were carried out to study the structural changes of the polymers in different temperatures. The measurements were done on both dilute solutions and on gelling semi dilute samples. We can see how the structure is affected by the length of the hydrophilic PEG block by comparing the SANS results from the two polymers.

5.4.1 Temperature effect on dilute polymeric samples

To understand the mechanism behind the gel network formation, we need to investigate the scattering results for a dilute solution for each of the polymers. In Figure 31 the scattering intensity (I(q)) is plotted against the scattering vector (q) in a log-log plot for a 1 wt% sample for each of the polymers. Different temperatures are indicated by different colours in Figure 31. The solid points represent heating, whilst the hollow points represent cooling.

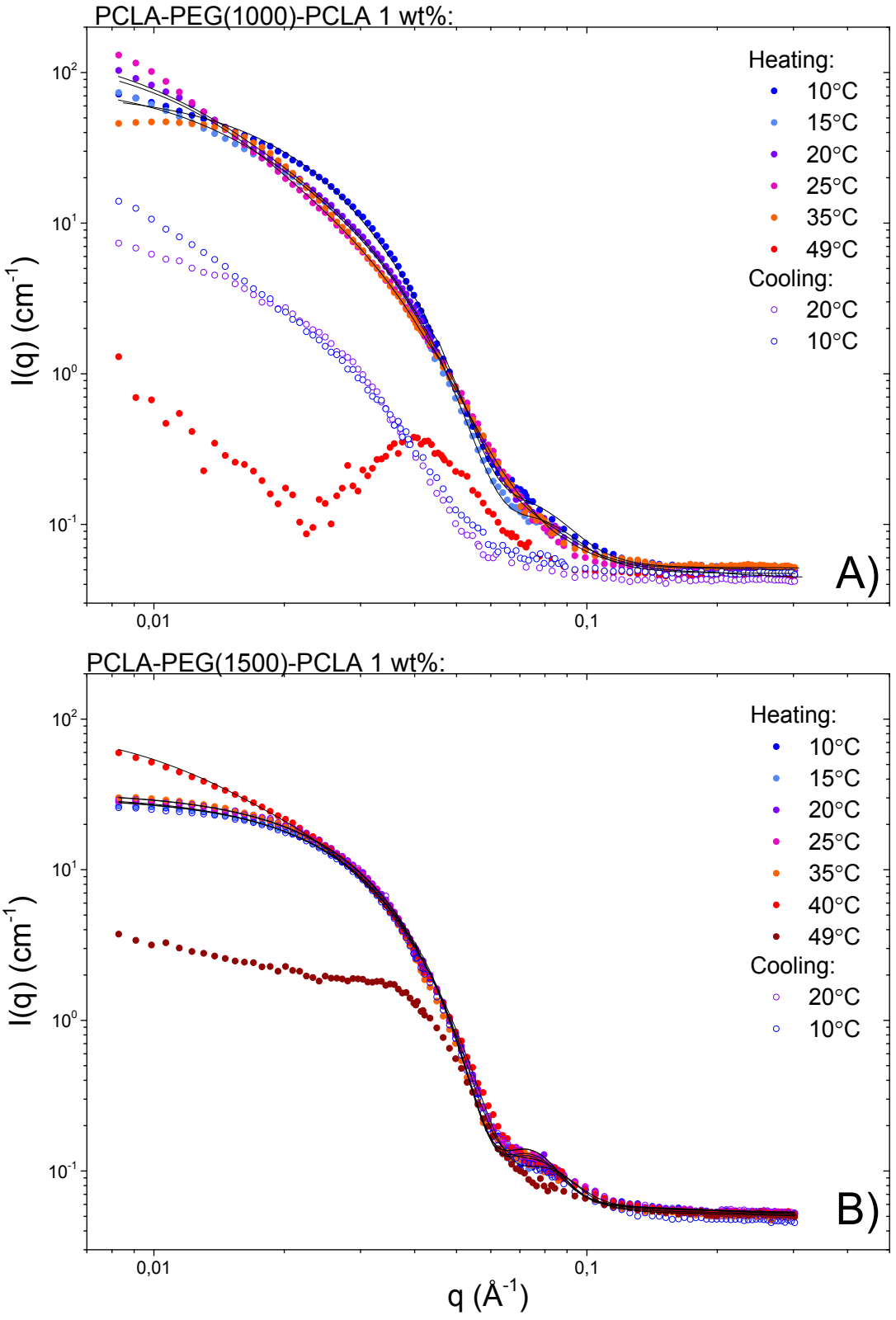

Figure 31. Scattered intensity plotted versus the scattering vector q for A) PCLA-PEG(1000)-PCLA 1 wt% and B) PClA-PEG(1500)-PCLA 1 wt% samples at different temperatures. Black lines indicated that a worm-like cylindrical micelle model has been fitted to the data for PCLA-PEG(1000)-PCLA and a core-shell sphere for PCLA-PEG(1500)-PCLA.

From Figure 31A) we see that the polymer with the shorter PEG spacer is strongly affected by temperature change. With increasing temperature the curves in the temperature range 10-35°C are quite similar in term of intensity, but the pattern changes significantly with increasing temperature. From 10°C to 25°C the slope in the Guinier region increases. One possible explanation for this is that the micellar structures become more elongated. We initially believed that this change in the structures could be explained by the formation of clusters of micelles. In PCLA-PEG(1000)-PCLA we believe that the PEG block is too short to form spherical flower like micelles. We therefore anticipated that this polymer system would form clusters of spherical core-shell micelles. To investigate this theory we tried fitting a cluster model to the scattering data for this polymer. The model is described in detail in Appendix A: Theoretical model for spherical core-shell micelle, and illustrated in Figure 32. After fitting the model to our data, we had to conclude that this model was not appropriate to explain our results. When we introduced a cluster of several micelles into the fitting, a significant correlation peak became visible. Such a correlation peak is not visible in our data. To remove the peak and fit the model to the data, the distance between each micelle (D) had to be significantly below the radius (Rm) of the micelles. This does not make sense because two micelles cannot be located in the same space. We therefor had to reconsider the hypothesis of the structures of this polymer at lower concentrations.

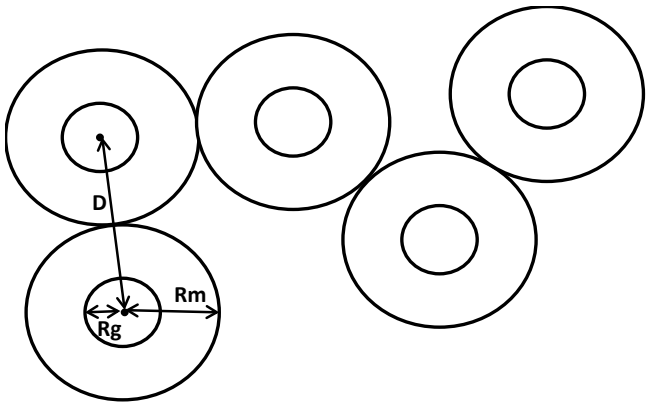

Figure 32. A schematic illustration of clustered core-shell structure. Rg is the radius of the core, while Rm is the radius of the whole micelle. D is the distance of the neighbouring micelles in a cluster. There are five micelles in the illustration but the number of micelles can be varied in the model.

After trying both an ellipsoidal model and a worm like cylinder model, we concluded that wormlike cylinders showed the best fit to our scattering data. For the lower temperature of 10-20°C we achieve a good fit with this model, but above this temperature the slope of the

Guinier region cannot be explained fully. A possible explanation for this steep slope is that it is caused by aggregation that is not included in the model. It might be that the sample did not have sufficient time to reach equilibrium prior to the measurement, resulting in a higher polydispersity. In these worm-like cylindrical micelles some of the PEG blocks loop around so that both hydrophobic blocks are in the core of the same micelle. However the PEG spacer is relatively short so some might be left in the solution. This is not favourable and might lead to connection of micelles (cluster formation). A sketch of worm-like cylindrical micelles is given in Figure 35, but the real picture is probably way more complex.

The numerical results from the model fitting to worm-like cylindrical micelles are shown in Table 4. From the numeric results we can see that the radius of the core decreases slightly with increasing temperature. This can be explained by shrinkage of the core consisting of the PCLA blocks as a function of temperature. The thickness of the shell however is constant at 2.13 ± 0.14 nm.

The flexibility of the chain is reported via the Kuhn length (a low Kuhn length is a result of highly flexible cylinders and vice versa). The Kuhn length has to be seen in context of the average contour length of the micelles. It is only when the contour length exceeds the Kuhn length that the micelles displays worm like features. It was shown during the analysis of the results that we could obtain good fits also with a larger Kuhn length, and it is therefore difficult to obtain some reliable information about the flexibility of the cylindrical chains. The values for Kuhn length that is given in Table 4 can therefore only be used as an indicator and in context of the other values. The problem with getting a reliable value for the Kuhn length from the modelling, is an indication that our system probably is too complex to be fully explained by the model. From these data we cannot fully conclude if the micelles are rigid or worm-like cylinders. In the future to be able to conclude on the structure of the micelles, we suggest that they should be investigated by for example transmission electron microscopy.

For the average chain length we identify a clear trend of increasing length with increasing temperature. We found a 3 times increase in the length of the cylindrical micelles with only a 10°C increase in temperature. This might be explained by the balance between all the forces that affects the systems. In the temperature range from 10°C to 20 °C we have a transition where it is energetically favourable for the system to form elongated cylinders. While we observe that the elongation process stops at approximately 20 degrees, because the average contour length of the micelles obtained for 20°C and 25°C is equal.

Table 4. Numerical results from fitting worm-like cylindrical micelle model.to the SANS data for PCLA-PEG(1000)-PCLA.

T (°C)	Radius core (Å)	Thickness shell (Å)	Kuhn length (Å)	Average contour length of micelles (Å)
10	56.02	19.43	336.26	244.28
15	54.34	22.78	342.83	431.38
20	53.40	21.08	313.55	717.87
25	52.03	21.80	238.36	717.6

At 35 °C we see a tendency to the formation of a correlation peak. The data could then no longer be explained with the worm-like cylindrical micelles model. In section 5.2 we identified a CP of 38°C for this polymer at 1 wt%. We can therefore anticipate that at 35 °C we probably have some changes in structure caused by the initial formation of aggregates. The curve from the 49°C measurement is shifted to a much lower intensity value indicating that the structures have been disrupted. For the highest temperature curve there is a clearly visible correlation peak at approximately q= 0.04. This peak indicates tight packing of structures with repeating distance of $\frac{2\pi}{q} = \frac{2\pi}{0{,}04} = 157$ Å . This peak can be explained by significant dehydration of the system. This supports the visual observation of precipitation at higher temperatures.

When the temperature is cooled down to first 20°C and then to 10°C the original shapes of the scattering curves returns, and thus the original structures is recovered. However you can notice a significantly lower overall intensity, this may be explained by aggregate formations at the highest temperature which is slowly being solubilised. We assume that if we had waited longer before measuring the sample, after cooling, the structures would be fully recovered for the whole sample.

For the PCLA-PEG(1500)-PCLA polymer (as seen in Figure 31B) the structure is more stable upon heating. The curves from the temperature range 10-35°C have approximately the same intensity and shape. The shapes of the curves resemble spherical particles and a core shell sphere model has therefore been fitted to the scattering data. The numerical results from the fittings are shown in Table 5. There is only a slight (but systematic) increase in the core radius from ca. 5.1 to 5.5 nm. We initially assumed that we would find the same shrinking of the

core for this polymer as we observed in PCLA-PEG(1000)-PCLA. One possible explanation of the expanding core radius is a morphological change from spheres to ellipsoids. This should be investigated further to understand the full explanation.

The shell thickness is constant at 2.77 ± 0.12 nm.

Table 5. Numerical results from fitting a spherical core-shell micelle model to the SANS data for PCLA-PEG(1500)-PCLA.

T (°C)	Radius core (Å)	Thickness shell (Å)	Comments
10	50.67	29.61	Sphere
15	52.72	27.72	"
20	54.31	26.53	"
25	54.24	26.97	"
35	55.63	27.86	"
40	40.58	25.02	Cylinder

Because this polymer has a longer PEG spacer, we suppose that the polymer chains might be able to make a complete loop so that both hydrophobic end blocks are situated in the core of the same micelle. These micelles can be described as being flower-like as illustrated in Figure 35. The packing parameter is lower for this polymer than for PCLA-PEG(1000)-PCLA. This is because the area of the hydrophilic group increases with increasing PEG spacer which makes a spherical shape more favourable.

It is more difficult to compare the numerical data obtained from fitting two different models to the scattering data for the two polymer systems, than with a system where both polymers could have been explained by the same model. It is also not proven that the models fully explain the polymer systems considering that the reality probably is even more complex. However from the data that was obtained it is shown that the micelles formed by PCLA-PEG(1500)-PCLA has a thicker shell than the cylindrical micelles formed by PCLA-PEG(1000)-PCLA. This can be directly linked to the difference in the length of the hydrophilic PEG block which constitutes the shell of the micelles.

Upon heating to 40 °C the pattern from PCLA-PEG(1500)-PCLA changes significantly, and the fit shows a somewhat smaller core (4.1nm) but a shell which is nearly the same as before

(2.5 nm). Here we assume a cylinder-like model because the slope of the curve in the Guinier region resembles elongated structures.

At 49°C the structure has been partly disrupted. The plateau starting at higher q indicates smaller structures. Here we assume that we have gotten a phase separation with sedimentation. This can be compared with a CP of 52°C that was determined by turbidity measurements.

When cooling the sample the original shapes are recovered, with no signs of any aggregation or degradation. The reason for this process being faster than for the PCLA-PEG(1000)-PCLA polymer is that the latter polymer is more water soluble (longer hydrophilic block).

5.4.2 Temperature effects of semi dilute polymeric samples

Because we now have a better picture of the structure of the polymers in dilute solutions, we can explain the behaviour of the system at higher concentrations. Firstly, we will look further into the scattering data from a semi dilute system of 20 wt% (Figure 33). Her we can see the structural changes for the sample in the temperature range were we observed a gel network from the tube tilting method (Figure 23).

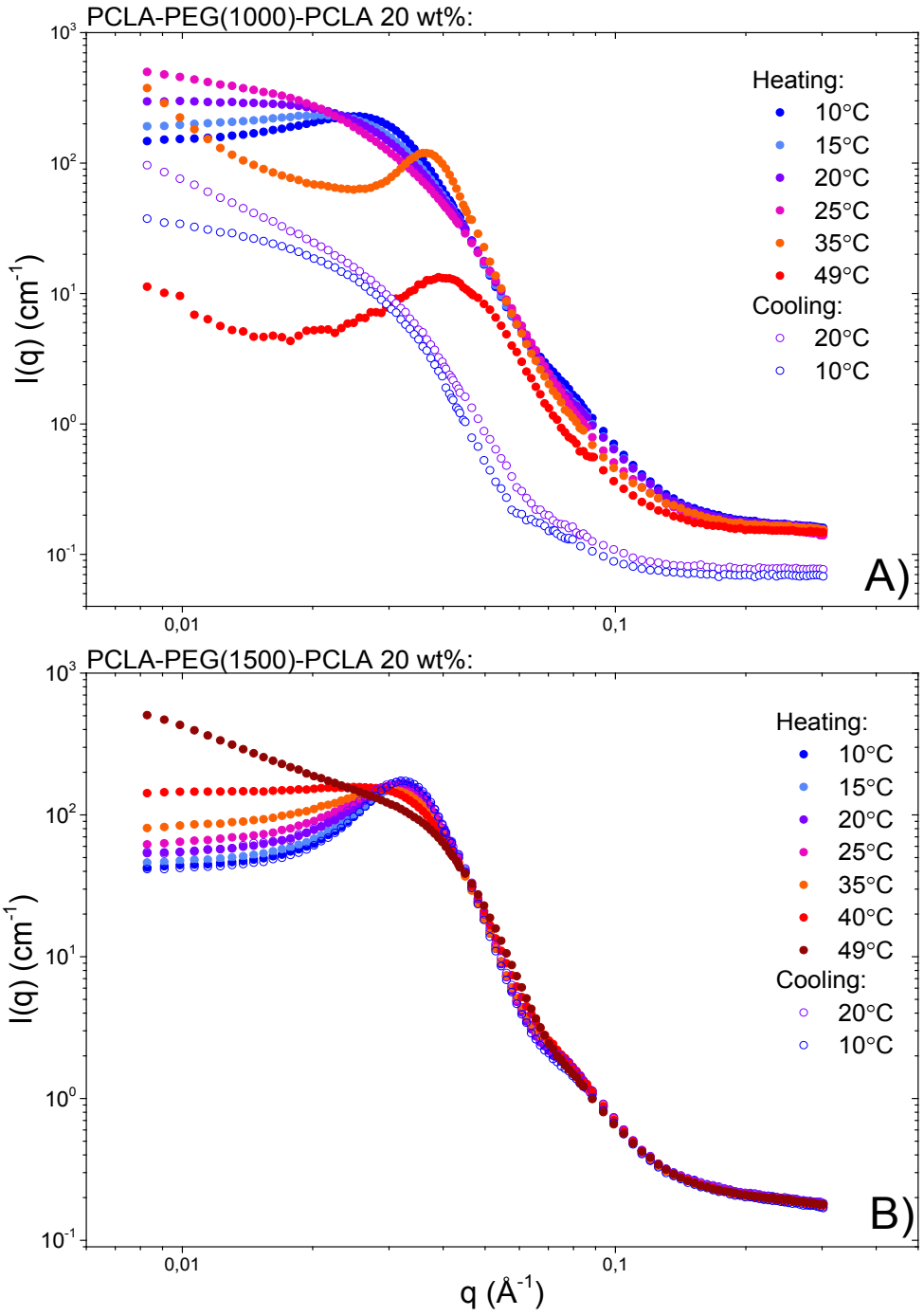

Figure 33. Scattered intensity plotted versus the scattering vector q for A) PCLA-PEG(1000)-PCLA 20 wt% and B) PClA-PEG(1500)-PCLA 20 wt% samples at different temperatures.

For the PCLA-PEG(1000)-PCLA polymer we observe a weak correlation peak indicating interaction between entities at low temperature (10°C). The scattering curve alone does not give us sufficient information to conclude with gel formation at this temperature. This is because we don't know if the interactions between the micelles are connected through the whole sample (percolation). These results hence have to be used in conjunction with for example rheology and tube-tilting methods to be able to draw conclusions about gelation. From the phase diagram (Figure 23) we observed a gel forming at approximately 10 °C, and an increase in dynamic viscosity at the same temperature from rheology. From analysing the dilute sample we concluded that the polymer self-assembled into worm-like cylindrical micelles. In the semi dilute sample we can anticipate that with increasing temperature, these worm-like cylindrical micelles grow in length and become more entangled. There might also be some bridging between the flexible cylinders causing a stronger network. These features will explain the increase in dynamic viscosity and the observation of a gel network. The polymer chains have a repeating distance of 233 Å ($\frac{2\pi}{q} = \frac{2\pi}{0{,}027\text{Å}^{-1}} = 232{,}71\text{Å}$). One can imagine that this might be the mesh size in the worm-like-cylinder network that is formed.

With increasing temperature there are large changes in the pattern and we observe an elongation of structures, explained by growth of the micelles (long micelles/rods) [47]. The correlation peak becomes less visible. We suppose that this is caused by several micelles aggregating to larger clusters because of the increased hydrophobicity with increasing temperature. The distance between each of these clusters become larger and the correlation peak becomes less visible.

The results for 20 wt% PCLA-PEG(1000)-PCLA is shown in a semilogarithmic plot in Figure 34. The scattering profile for 15, 20 and 25 °C has been multiplied by 5, 5^2, and 5^3 respectively, to achieve a vertical shift of the data. Here we see a clear trend. When increasing the temperature the correlation peak broadens. This indicates that the long-range order is disrupted with higher temperature. This might be explained by thermally induced hydrophobic attraction. This result can be compared with the behaviour identified for an ABA type PEO-PLGA-PEO polymer by M. J. Park and K. Char [54].

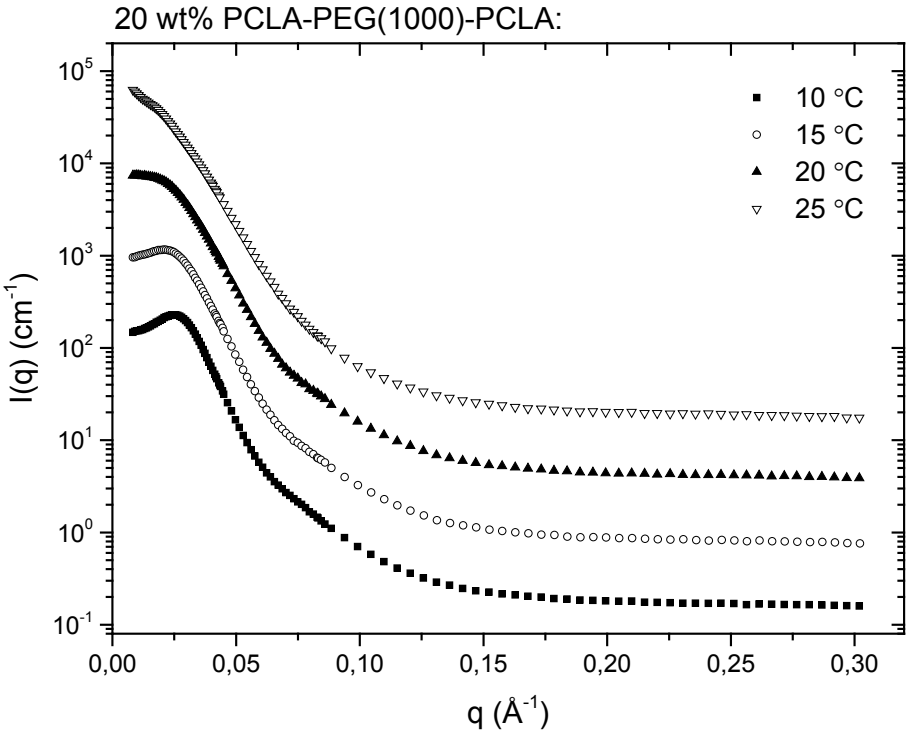

Figure 34. The SANS profile og an aqueous 20 wt% solution of PCLA-PEG(1000)-PCLA upon heating from 10°C to 25°C. The curves have been shifted for clarity.

The sample undergoes drastic changes at 35 °C. Here we probably see the formation of large aggregates with a repeating distance of 0,035Å^{-1} ($\frac{2\pi}{q} = \frac{2\pi}{0{,}037\text{Å}^{-1}} = 169{,}7\text{Å}$) as calculated from the correlation peak. At further heating to 49°C the structure has been partly disrupted and the correlation peak has moved to q=0,039Å^{-1}, implying a shorter repeating distance of 161.1 Å ($\frac{2\pi}{q} = \frac{2\pi}{0{,}039\text{Å}^{-1}}$). This can be explained by phase separation, and sedimentation of aggregates resulting in a lower intensity.

Upon cooling the pattern returns to the original shape but with somewhat lower intensity than before, the same trend as for the dilute sample of this polymer (Figure 31A). This is probably due to not all material recovering after heating. The pattern is now characteristic for individual micelles.

For the PCLA-PEG(1500)-PCLA polymer we observed individual spherical flower-like micelles at the lower concentration. In a semi-dilute sample we see a strong interaction at low temperature (Figure 33B). The correlation peak becomes smaller upon increasing temperature. This can be explained by the formation of aggregates or increased thermal

motion of micelles. At 40 °C the correlation peak has nearly disappeared indicating more independent entities. During heating of the sample to the highest temperature of 49 °C, the system undergoes a dramatic change. The nanostructure now resembles that of highly elongated structures (low-q slope of minus one). Upon cooling the original shape is recovered as for the 1 wt% sample of the same polymer.

By comparing the SANS results from the two polymers, we can get an impression of how altering the length of the hydrophilic PEG spacer affects the structure of the micelles. At lower temperature (10 °C) we see an indication of a tighter and more well-defined network when increasing the PEG length. The correlation peak is more defined and is shifted to higher q indicating smaller distance between entities. An interesting change is observed after increasing the temperature to 35 °C. The correlation peak is visible at a higher q for the polymer with the shorter PEG length, indicating shorter distance between entities. Here we anticipate that the PCLA-PEG(1000)-PCLA system changes from having a more open network than PCLA-PEG(1500)-PCLA, to a tighter network than the latter polymer. The polymer with the longer PEG length is quite stable in this temperature range, so this change is mainly due to reorganisation within the PCLA-PEG(1000)-PCLA system.

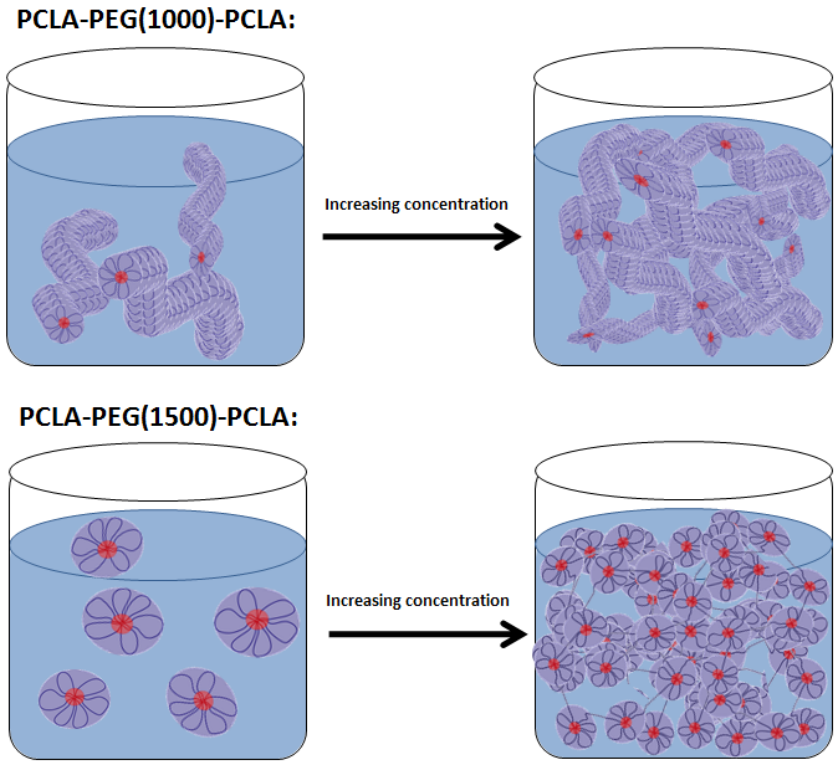

Figure 35. Illustration of the hypothesis for micellar structure and gelation of both PCLA-PEG(1000)-PCLA and PCLA-PEG(1500)-PCLA.

From comparing the SANS results for the two polymers, we can conclude that the shorter PEG spacer gives more room for tuning properties of the system because the nanostructure changes more with increasing temperature. We observed this trend also in the dynamic viscosity as a function of temperature plots (Figure 29). The dynamic viscosity of the PCLA-PEG(1000)-PCLA polymer underwent larger changes with temperature than the polymer with the longer PEG spacer. For the latter polymer we believe that at lower concentrations we have stable spherical flower-like micelles that occupy a small effective volume. These micelles don't substantially interact with each other, resulting in a low viscosity (illustrated in Figure 35). When we reach the critical concentration for gelation the micelles will be more packed together and there will be bridging of micelles. Here we also observe some temperature effects on the viscosity. However when we reach the concentration of 30 wt% of the polymer with the longer PEG spacer, the dynamic viscosity is steadily high. This can be explained by a jamming effect. Here the concentrations of the micelles (that are formed already at lower temperature) are relatively high. The micelles are jammed together. This effect combined with the bridges formed between the micelles, lead to a high dynamic viscosity over a wide temperature range.

Pharmaceutical application related to the structure:

From characterising the structures of the polymeric samples via small angle neutron scattering, we have obtained a more accurate image of the gelation process. We now know that a gel can be formed at a lower concentration for the polymer with the shorter PEG spacer because of the elongated micellar structure. From a drug formulation perspective we prefer to be able to use a small amount of excipients. This is related to costs, stability and toxicity [8].

We have also learnt that the PCLA-PEG(1000)-PCLA polymer undergoes larger changes with temperature, while the polymer with the longer PEG spacer is more stable. This has both positive and negative consequences related to drug delivery application. To achieve our goal of an *in situ* gelling implant we need a system that is highly influenced by temperature changes in the appropriate range. As we determined from rheology, both systems undergoes gelation at a lower temperature than we are aiming for. What we however have not discussed, is how the temperature for gel melting and phase separation affects the pharmaceutical usability. We see from both cloud point analysis and the small angle scattering results, that

the semi dilute samples of PCLA-PEG(1000)-PCLA phase separates bellow the physiological temperature. The polymer with the longer PEG spacer has a higher CP, but visual observations from the tube inverting method indicate a gel to sol phase transition around the physiological temperature. These tests have been performed in pure water. The body fluids have a much more complex composition, and we can therefore anticipate that this will change some of the measured features. We might have to consider changing the chemical composition of the polymer systems to be able to use this kind of polymer as a drug delivery system. In this work the balance between large enough hydrophobic groups, to prevent a too quick degradation, and a large enough hydrophilic mid group, to secure solubility and a high CP, has to be further investigated and developed.

5.4.3 Comparing different concentrations of PCLA-PEG(1000)-PCLA

For the PCLA-PEG(1000)-PCLA polymer we observed from the rheology and the phase diagram (Figure 23), that this polymer can form a gel-like sample at a lower concentration than the polymer with the longer PEG spacer. This can be explained by the structural differences of these polymers. Because the PCLA-PEG(1000)-PCLA polymer is elongated as flexible cylindrical micelles, it requires a lower concentration to form a percolated network. To investigate how the structures in this polymer system are affected by increasing concentration, we have plotted the scattering data from this polymer at 5 different concentrations at 10 °C (Figure 36). The low temperature of 10 °C is interesting to investigate for this polymer because we observe gelation around this temperature.

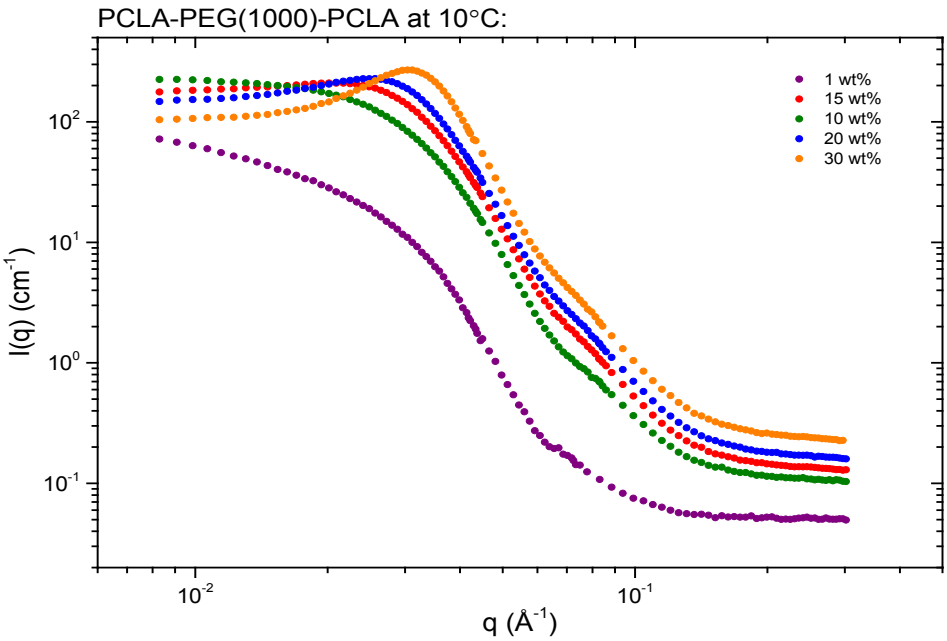

Figure 36. Scattered intensity versus the scattering vector for PCLA-PEG(1000)-PCLA at 10°C at the indicated concentrations.

From the plot in Figure 36 we can see that a correlation peak is visible at 15 wt% an above. This indicates interactions between the entities. The correlation peaks shift to higher q with increasing concentration of the PCLA-PEG(1000)-PCLA polymer. This is explained by the fact that the distance between the entities shortens when you increase the amount of polymer, as expected. Bellow 15 wt% only weak interactions are present (individual entities). We don't observe gelation under this concentration either. The whole set of curves at every temperature for all the concentrations are attached in appendix D.

5.5 The effect of phosphate buffer of pH 7,4

All the experiments reported above were performed in Mili-Q water, because we wanted to investigate the pure temperature effect without the complications of salts and pH first. The results from our experiments in water suggest that the polymer system behaves in a complex way. The gelation temperature is too low for being used as a drug formulation that gels *in situ*. The situation for the polymer system in the human body is even more complex. In the body we find factors like salts, pH effects and pressure. We therefore thought that a natural step for further research was to perform rheology experiments in a phosphate buffer with pH 7.4.

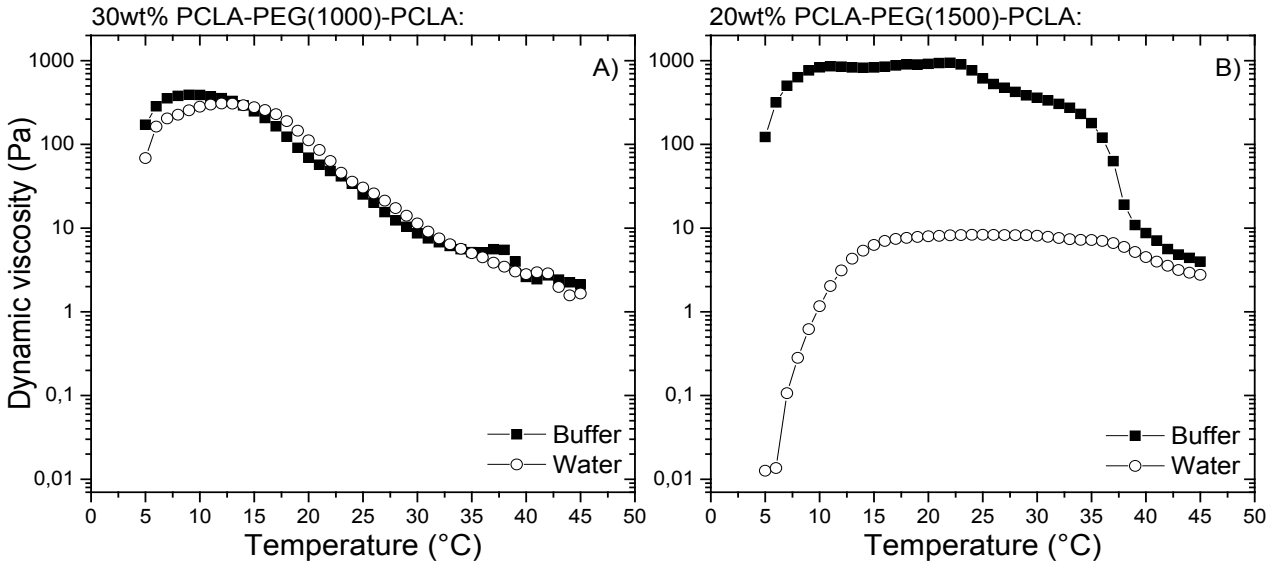

Figure 37. The dynamic viscosity of A) 30 wt% of PCLA-PEG(1000)-PCLA and B) 20wt% PCLA-PEG(1500)-PCLA in phosphate buffer of pH 7,4 and in water as indicated, plotted against temperature.

As observed in Figure 37A) we could not see a large difference between polymeric solutions in buffer and in water for PCLA-PEG(1000)-PCLA. The curve is shifted slightly to the left (lower temperature). The gel point determined for the polymer in buffer is approximately 5°C. This is in agreement with the dynamic viscosity curve being slightly shifted to lower temperature.

For the polymer with the longer PEG spacer the difference between the two solvents is much larger (Figure 37B). The polymer dissolved in water has a quite stable dynamic viscosity of ca. 8.2 Pa from 16-37°C, while the same polymer dissolved in phosphate buffer with a pH of 7,4 has a peak value of 943 Pa at 22°C. The curve has a plateau from approximately 10- 23 °C and declines slowly after that.

The lactic acid monomer has a carboxyl group. The group becomes an ester group when polymerised. The lactic acid is randomly copolymerised with caprolactone in our polymer. Because this is random, we cannot know if the end group is a LA monomer with a remaining carboxyl group. We can therefore expect that there might have a pH effect. The alteration of pH might affect the structure of the polymer, but this has not been verified [55]. Using pH sensitive groups to cap the PCLA-PEG-PCLA polymers has been widely investigated [23, 56-62]. They utilize pH sensitivity for adjusting the gel properties of the system. The pH effect on our polymer needs to be investigated further. The possibility of using a pH sensitive end group might be an option for further development of this project.

However we suggest that the change in dynamic viscosity is caused by the addition of salts, not by the alteration of pH. We suppose that this is related to the Hofmeister effect. The polymer becomes less water soluble because of the addition of phosphate, which is a kosmotrope. This will make the micelles aggregate at a lower temperature resulting in a higher dynamic viscosity. We can expect that this effect is higher for the polymer with the longer PEG spacer because the structure here is more disrupted by the salts. The flower-like micelles are stable in water, but when we add salts to the solution the PEG becomes less water soluble. When the hydrophilic block becomes less water soluble, the micelles become destabilised. As discussed earlier these polymer chains forms bridges between micelles because the PEG spacer is longer. We believe that the addition of salts results in an increase in the amount of bridges between the micelles. This will drastically increase the dynamic viscosity. The PCLA-PEG(1000)-PCLA polymer have a shorter PEG group, so that forming the stable flower-like micelles is not possible. This polymer is already forming clusters of cylinders in pure water with a high aggregation number, and is therefore not affected noticeable by the addition of salt.

From a drug formulation perspective we would have preferred that the gelation had been shifted to a higher temperature with the addition of salts, instead we observe the opposite effect. The phenomena we have identified from rheology needs to be further researched. We could for example assume that the cloud point of the solutions will be shifted towards lower temperature. This can be proven by doing turbidity measurements of the polymer in buffer. The effect of salt on the structures of the micelles and polymeric network, can be investigated by performing small angle neutron scattering experiments of samples with added salts.

6 Conclusions

The main objective of this study was to examine temperature-responsive amphiphilic triblock copolymers intended for *in situ* gelling drug delivery systems. After a screening of different polymers, two promising candidates of PCLA-PEG-PCLA with altering length of the mid spacer were chosen.

Via the tube tilting method approximate gel point, gel melting temperature and cloud point were determined. This observational study showed that with increasing PEG spacer the gel phase reaches a wider temperature range, while the polymer with the shorter PEG spacer formed a gel at a lower concentration. From turbidity measurement it was showed that the CP shifts to higher temperatures with decreasing concentration and increasing PEG spacer. The small angle neutron scattering results supports these findings.

From the rheology measurements it was only possible to obtain a critical gel point for the polymer with the shorter PEG spacer at the highest concentration. The gel point obtained was lower than the optimal gel point considering *in situ* gelling drug delivery application. The dynamic viscosity was higher for the polymer with the longer PEG spacer at the highest concentration; however this polymer was shown to be less temperature responsive over the interesting temperature range. Analysing small angle scattering data for these polymers lead to one possible explanation for the rheological features. A worm like cylindrical micelle model was fitted to the data for the polymer with the shorter hydrophilic spacer, while the other polymer could be explained by a spherical core-shell model. This difference in morphology might be related to the packing parameter decreasing with increasing area of the hydrophilic group.

When doing rheology experiments in phosphate buffer with pH 7.4, the PCLA-PEG(1500)-PCLA sample shows a drastic increase in dynamic viscosity with addition of salts. This trend can be related to the Hofmeister effect.

From this study it has been shown that PCLA-PEG-PCLA may be an interesting candidate for *in situ* gelling drug delivery of microparticles loaded with Naltrexone. However, this polymer system has proven to be very complex. Further studies should focus on optimising the overall chemical composition of the polymer for gelation in the right temperature range, and adequate gel strength.

References

1. Olsen, L., et al., *Plasma concentrations during naltrexone implant treatment of opiate-dependent patients.* British journal of clinical pharmacology, 2004. **58**(2): p. 219-222.
2. Calejo, M.T., et al., *Microparticles based on hydrophobically modified chitosan as drug carriers.* Journal of Applied Polymer Science, 2014. **131**(7): p. 40055.
3. Kjøniksen, A.-L., et al., *Stabilization of Pluronic Gels by Hydrophobically Modified Hydroxyethylcellulose.* International Journal of Polymeric Materials and Polymeric Biomaterials, 2015. **64**(2): p. 76-83.
4. Kjøniksen, A.L., et al., *Stabilization of pluronic gels in the presence of different polysaccharides.* Journal of Applied Polymer Science, 2014. **131**(13).
5. Calejo, M.T., et al., *In vitro cytotoxicity of a thermoresponsive gel system combining ethyl (hydroxyethyl) cellulose and lysine-based surfactants.* Colloids and Surfaces B: Biointerfaces, 2013. **102**: p. 682-686.
6. Calejo, M.T., et al., *Interactions between ethyl (hydroxyethyl) cellulose and lysine-based surfactants in aqueous media.* European Polymer Journal, 2012. **48**(9): p. 1622-1631.
7. Calejo, M.T., et al., *Thermoresponsive hydrogels with low toxicity from mixtures of ethyl (hydroxyethyl) cellulose and arginine-based surfactants.* International journal of pharmaceutics, 2012. **436**(1): p. 454-462.
8. Aulton, M.E., ed. *Aulton's pharmaceutics: the design and manufacture of medicines*. 3rd ed. 2007, Churchill Livingstone: Edinburgh. 716.
9. Tiwari, G., et al., *Drug delivery systems: an updated review.* International journal of pharmaceutical investigation, 2012. **2**(1): p. 2.
10. Gil, E.S. and Hudson, S.M., *Stimuli-reponsive polymers and their bioconjugates.* Progress in polymer science, 2004. **29**(12): p. 1173-1222.
11. Lazzari, M., Liu, G. and Lecommandoux, S., eds. *Block Copolymers in Nanoscience*. 2006, Wiley-VCH: Weinheim. 427.
12. Dormidontova, E.E., *Role of competitive PEO-water and water-water hydrogen bonding in aqueous solution PEO behavior.* Macromolecules, 2002. **35**(3): p. 987-1001.
13. Nyström, B. and Walderhaug, H., *Dynamic Viscoelasticity of an Aqueous System of a Poly (ethylene oxide)-Poly (propylene oxide)-Poly (ethylene oxide) Triblock Copolymer during Gelation.* The Journal of Physical Chemistry, 1996. **100**(13): p. 5433-5439.
14. Fuertges, F. and Abuchowski, A., *The clinical efficacy of poly (ethylene glycol)-modified proteins.* Journal of controlled release, 1990. **11**(1): p. 139-148.
15. Florence, A.T. and Attwood, D., *Physicochemical principles of pharmacy*. 5th ed. 2011, London: Pharmaceutical Press.
16. Goldberg, D., *A review of the biodegradability and utility of poly (caprolactone).* Journal of environmental polymer degradation, 1995. **3**(2): p. 61-67.
17. Bae, S.J., et al., *Thermogelling poly (caprolactone-b-ethylene glycol-b-caprolactone) aqueous solutions.* Macromolecules, 2005. **38**(12): p. 5260-5265.
18. Moon, H.J., et al., *Temperature-responsive compounds as in situ gelling biomedical materials.* Chemical Society Reviews, 2012. **41**(14): p. 4860-4883.
19. Garlotta, D., *A literature review of poly (lactic acid).* Journal of Polymers and the Environment, 2001. **9**(2): p. 63-84.

20. Zhang, Z., et al., *Biodegradable and thermoreversible PCLA–PEG–PCLA hydrogel as a barrier for prevention of post-operative adhesion.* Biomaterials, 2011. **32**(21): p. 4725-4736.
21. Jiang, Z., Deng, X. and Hao, J., *Thermogelling hydrogels of poly (ε-caprolactone-co-D, L-lactide)–poly (ethylene glycol)–poly (ε-caprolactone-co-D, L-lactide) and poly (ε-caprolactone-co-L-lactide)–poly (ethylene glycol)–poly (ε-caprolactone-co-L-lactide) aqueous solutions.* Journal of Polymer Science Part A: Polymer Chemistry, 2007. **45**(17): p. 4091-4099.
22. Bramfeldt, H., Sarazin, P. and Vermette, P., *Characterization, degradation, and mechanical strength of poly (D, L-lactide-co-ϵ-caprolactone)-poly (ethylene glycol)-poly (D, L-lactide-co-ϵ-caprolactone).* Journal of Biomedical Materials Research Part A, 2007. **83**(2): p. 503-511.
23. Sandker, M.J., et al., *In situ forming acyl-capped PCLA–PEG–PCLA triblock copolymer based hydrogels.* Biomaterials, 2013. **34**(32): p. 8002-8011.
24. Israelachvili, J.N., Mitchell, D.J. and Ninham, B.W., *Theory of self-assembly of hydrocarbon amphiphiles into micelles and bilayers.* Journal of the Chemical Society, Faraday Transactions 2: Molecular and Chemical Physics, 1976. **72**: p. 1525-1568.
25. Zhu, J., et al., *Disk-cylinder and disk-sphere nanoparticles via a block copolymer blend solution construction.* Nat Commun, 2013. **4**.
26. Rosiak, J.M. and Yoshii, F., *Hydrogels and their medical applications.* Nuclear Instruments and Methods in Physics Research Section B: Beam Interactions with Materials and Atoms, 1999. **151**(1): p. 56-64.
27. Lee, K.Y. and Mooney, D.J., *Hydrogels for tissue engineering.* Chemical reviews, 2001. **101**(7): p. 1869-1880.
28. Hoffman, A.S., *Hydrogels for biomedical applications.* Advanced drug delivery reviews, 2002. **54**(1): p. 3-12.
29. Gennes, P.-G.d., *Scaling concepts in polymer physics*. 1st ed. 1979, Ithaca, N.Y: Cornell University Press. 324.
30. Hillery, A.M., Lloyd, A.W. and Swarbrick, J., eds. *Drug delivery and targeting for pharmacists and pharmaceutical scientists*. 2001, Taylor & Francis: London.
31. Lee, D.S., et al., *Novel Thermoreversible Gelation of Biodegradable PLGA-block-PEO-block-PLGA Triblock Copolymers in Aqueous Solution.* Macromolecular rapid communications, 2001. **22**(8): p. 587-592.
32. Hofmeister, F., *Zur Lehre von der Wirkung der Salze.* Naunyn-Schmiedeberg's Archives of Pharmacology, 1888. **24**(4): p. 247-260.
33. Kunz, W., Henle, J. and Ninham, B.W., *'Zur Lehre von der Wirkung der Salze'(about the science of the effect of salts): Franz Hofmeister's historical papers.* Current Opinion in Colloid & Interface Science, 2004. **9**(1): p. 19-37.
34. Fanaian, S., et al., *Effects of Hofmeister anions on the flocculation behavior of temperature-responsive poly (N-isopropylacrylamide) microgels.* Colloid and Polymer Science, 2012. **290**(16): p. 1609-1616.
35. Kjøniksen, A.-L., et al., *Association in aqueous solutions of a thermoresponsive PVCL-g-C11EO42 copolymer.* Macromolecules, 2005. **38**(3): p. 948-960.
36. Barnes, H.A., Hutton, J.F. and Walters, K., *An introduction to rheology*. Rheology series. Vol. 3. 1989, Amsterdam: Elsevier.
37. Larson, R.G., *The structure and rheology of complex fluids*. Topics in chemical engineering, ed. Gubbins, K.E. 1999, New York: Oxford University Press. 663.
38. Barnes, H.A., Hutton, J.F. and Walters, K., *An introduction to rheology*. Rheology series. Vol. 3. 1989, Amsterdam: Elsevier. 199.

39. Grosberg, A.Y. and Khokhlov, A.R., *Giant molecules: here, there, and everywhere,*. 2nd ed. Philosophical, Historical, Educational and Interdisciplinary Studies of Chemistry. Vol. 14. 2012, Dordrecht: World Scientific Publishing. 322.
40. Winter, H.H. and Chambon, F., *Analysis of linear viscoelasticity of a crosslinking polymer at the gel point.* Journal of Rheology, 1986. **30**(2): p. 367-382.
41. Winter, H., *Can the gel point of a cross-linking polymer be detected by the G'–G "crossover?* Polymer Engineering & Science, 1987. **27**(22): p. 1698-1702.
42. Chambon, F. and Winter, H.H., *Stopping of crosslinking reaction in a PDMS polymer at the gel point.* Polymer Bulletin, 1985. **13**(6): p. 499-503.
43. Holly, E.E., et al., *Fourier transform mechanical spectroscopy of viscoelastic materials with transient structure.* Journal of non-newtonian fluid mechanics, 1988. **27**(1): p. 17-26.
44. Richtering, H., et al., *Physical gelation of a bacterial thermoplastic elastomer.* Macromolecules, 1992. **25**(9): p. 2429-2433.
45. Rubinstein, M. and Dobrynin, A.V., *Associations leading to formation of reversible networks and gels.* Current opinion in colloid & interface science, 1999. **4**(1): p. 83-87.
46. Higgins, J.S. and Benoît, H., *Polymers and neutron scattering*. Oxford series on neutron scattering in condensed matter. 1994, Oxford: Clarendon Press 436.
47. Hammouda, B., *The SANS Toolbox.* NIST Center for Neutron Research,, 2008.
48. Abe, A., et al., *Controlled Polymerization and Polymeric Structures: Flow Microreactor Polymerization, Micelles Kinetics, Polypeptide Ordering, Light Emitting Nanostructures*. Flow Microreactor Polymerization, Micelles Kinetics, Polypeptide Ordering, Light Emitting Nanostructures. Vol. 259. 2013, Cham: Springer International Publishing, Cham.
49. Khorshid, N.K., *Novel Structural Changes During Temperature-Induced Self-Assembling and Gelation in Aqueous Solutions of the Copolymer PLGA1170-PEGn-PLGA1170*, in *Department of Chemistry*. 2013, University of Oslo: Oslo.
50. Jensen, G.V., et al., *Monitoring the Transition from Spherical to Polymer-like Surfactant Micelles Using Small-Angle X-Ray Scattering.* Angewandte Chemie, 2014. **126**(43): p. 11708-11712.
51. Sommer, C., Pedersen, J.S. and Stein, P.C., *Apparent specific volume measurements of poly (ethylene oxide), poly (butylene oxide), poly (propylene oxide), and octadecyl chains in the micellar state as a function of temperature.* The Journal of Physical Chemistry B, 2004. **108**(20): p. 6242-6249.
52. Kjøniksen, A.-L. and Nyström, B., *Effects of polymer concentration and cross-linking density on rheology of chemically cross-linked poly (vinyl alcohol) near the gelation threshold.* Macromolecules, 1996. **29**(15): p. 5215-5222.
53. Kjøniksen, A.-L., Nyström, B. and Lindman, B., *Dynamic viscoelasticity of gelling and nongelling aqueous mixtures of ethyl (hydroxyethyl) cellulose and an ionic surfactant.* Macromolecules, 1998. **31**(6): p. 1852-1858.
54. Park, M.J. and Char, K., *Gelation of PEO-PLGA-PEO triblock copolymers induced by macroscopic phase separation.* Langmuir, 2004. **20**(6): p. 2456-2465.
55. Chang, G., et al., *A delicate ionizable-group effect on self-assembly and thermogelling of amphiphilic block copolymers in water.* Polymer, 2009. **50**(25): p. 6111-6120.
56. Petit, A., et al., *Modulating rheological and degradation properties of temperature-responsive gelling systems composed of blends of PCLA–PEG–PCLA triblock copolymers and their fully hexanoyl-capped derivatives.* Acta biomaterialia, 2012. **8**(12): p. 4260-4267.

57. Shim, W.S., et al., *Biodegradability and biocompatibility of a pH-and thermo-sensitive hydrogel formed from a sulfonamide-modified poly (ε-caprolactone-co-lactide)–poly (ethylene glycol)–poly (ε-caprolactone-co-lactide) block copolymer.* Biomaterials, 2006. **27**(30): p. 5178-5185.
58. Nguyen, M.K. and Lee, D.S., *Injectable biodegradable hydrogels.* Macromolecular bioscience, 2010. **10**(6): p. 563-579.
59. Tang-na, H., et al., *pH and temperature sensitive properties and drug release in vitro of OSM-PCLA-PEG-PCLA-OSM block copolymer hydrogel.* Journal of Shenyang Pharmaceutical University, 2009. **5**: p. 004.
60. Shim, W.S., et al., *pH-and temperature-sensitive, injectable, biodegradable block copolymer hydrogels as carriers for paclitaxel.* International journal of pharmaceutics, 2007. **331**(1): p. 11-18.
61. Shim, W.S., Kim, S.W. and Lee, D.S., *Sulfonamide-based pH-and temperature-sensitive biodegradable block copolymer hydrogels.* Biomacromolecules, 2006. **7**(6): p. 1935-1941.
62. Petit, A., et al., *Effect of polymer composition on rheological and degradation properties of temperature-responsive gelling systems composed of acyl-capped PCLA-PEG-PCLA.* Biomacromolecules, 2013. **14**(9): p. 3172-3182.
63. Guinier, A., et al., *Small-Angle Scattering of X.* Rays, 1955: p. 167-195.
64. Pedersen, J.S. and Schurtenberger, P., *Scattering Functions of Semiflexible Polymers with and without Excluded Volume Effects.* Macromolecules, 1996. **29**(23): p. 7602-7612.
65. Daoud, M. and Cotton, J., *Star shaped polymers: a model for the conformation and its concentration dependence.* Journal de Physique, 1982. **43**(3): p. 531-538.
66. Pedersen, J.S. and Svaneborg, C., *Scattering from block copolymer micelles.* Current opinion in colloid & interface science, 2002. **7**(3): p. 158-166.
67. Svaneborg, C. and Pedersen, J.S., *Block copolymer micelle coronas as quasi-two-dimensional dilute or semidilute polymer solutions.* Physical Review E, 2001. **64**(1): p. 010802.
68. Lund, R., et al., *Structural and thermodynamic aspects of the cylinder-to-sphere transition in amphiphilic diblock copolymer micelles.* Soft Matter, 2011. **7**(4): p. 1491-1500.
69. Beaucage, G., *Small-angle scattering from polymeric mass fractals of arbitrary mass-fractal dimension.* Journal of Applied Crystallography, 1996. **29**(2): p. 134-146.
70. Devanand, K. and Selser, J., *Asymptotic behavior and long-range interactions in aqueous solutions of poly (ethylene oxide).* Macromolecules, 1991. **24**(22): p. 5943-5947.

Appendix A: Theoretical model for spherical core-shell micelles

The theoretical model considers a two level structure of the scattering from micellar aggregates, to be made of BAB block copolymers in an A-selective solvent. The total scattering intensity as a function of scattering vector *Q* has the following general form:

$$I(Q) = \left(\frac{N}{V}\right)(\Delta SLD)^2 Vp^2 P(Q) \tag{13}$$

where *(N/V)* is the number density of particles, *ΔSLD* is the difference in scattering length density of the polymer compared to the solvent, and *Vp* is the volume of the particles. P(Q) is the form factor and is given by the following equation [63]:

$$P(Q) = \frac{scale}{V_s}\left[3V_c(\rho_c - \rho_s)\frac{[\sin(qr_c) - qr_c * \cos(qr_c)]}{(qr_c)^3} + 3V_s(\rho_s - \rho_{solv})\frac{[\sin(qr_s) - qr * cos(qr_s)]}{(qr_s)^3}\right]^2 + bkg \tag{14}$$

Here *scale* is a scale factor. V_s is the volume of the outer shell while V_c is the volume of the core. r_s is the radius of the shell and r_c is the radius of the core, while ρ_c, ρ_s and ρ_{solv} is the scattering length density of the shell, core and solvent respectively. Bkg is the background level.

Appendix B: Theoretical model for worm-like cylindrical micelles

The total scattering intensity as a function of scattering vector Q has the following general form for these worm-like cylindrical micelles:

$$I(Q) = \frac{N_{polymer}}{V * p_{worm}} * P_{cs-worm}(Q) \tag{15}$$

where $N_{polymer}/V$ is the number density of polymer molecules, p_{worm} is the aggregation number for the wormlike micelles.

It has been showed by G.V. Jensen et al.[50] that the form factor ($P_{cs,worm}(Q)$) for the worm-like micelles can be expressed by the following function:

$$P_{cs-worm}(Q) = [\Delta\rho_{corona} V_{tot} A_{cr}(QR_{tot}) + (\Delta\rho_{core} - \Delta\rho_{corona}) V_{core} A_{cr}(QR_{core})]^2 P_{chain}(Q, L, b) \tag{16}$$

Here $R_{core,}$ is the core radius of the micelles. The total radius is $R_{tot} = R_{core} + D$, were D is the shell thickness. $\Delta\rho$ is the contrast factor i.e. the difference in the scattering length density of the polymer compared to the solvent. L is the contour length of the cylinders and b is a Kuhn length. It is only for $L>b$ that the cylindrical micelles are worm-like. $L>b$, corresponds to a rod like, cylinder micelle. Volume of the micelle is $V_{tot}=\pi R_{tot}^2 L$, while volume of the core is $V_{core}=\pi R_{core}^2 L$. $A_{cr}(Q)$ is the scattering amplitude for the circular cross-section. $P_{chain}(q,L,B)$ is an expression for the scattering from the worm-like features in the longitudinal direction of the cylindrical micelles. The scattering can be written as a combination of the scattering from a rod of length L, and from a random-walk self-avoiding chain of length L and Kuhn length b. This was proven by analysing simulated scattering patterns from worm-like chains, by J. S. Pedersen and P. Schurtenberg[64].

Appendix C: Theoretical model for clustered micelles

The theoretical model considers a two level structure of the scattering from micellar aggregates, to be made of BAB block copolymers in an A-selective solvent. The total scattering intensity as a function of scattering vector *Q* has the following general form:

$$\frac{\mathrm{d}\Sigma}{\mathrm{d}\Omega}(Q) = \frac{\phi}{N_{\mathrm{agg}} \cdot V_p} \cdot P(Q) \cdot S(Q) \tag{17}$$

where *Φ* is the polymer volume, V is the volume of the micellar entity and N_{agg} denotes the number of aggregated chains per micelle. *P(Q)* is the normalised form factor *P(Q → 0),* and *S(Q)* the structure factor. The latter expresses the attractive forces as a result of the B-bridges resulting in larger clusters composed of several micelles.

The function *P(Q)* in Eq. 17 Appendix A: Theoretical model for spherical core-shell micellehas the form:

$$\begin{aligned} P(Q) = {} & \Delta\varrho_{\mathrm{C_n}}^2 \cdot N_{\mathrm{agg}}^2 \cdot V_{\mathrm{C_n}}^2 \cdot A_{\mathrm{C_n}}^2(Q) \\ & + \Delta\varrho_{\mathrm{PEO}}^2 \cdot N_{\mathrm{agg}} \cdot (N_{\mathrm{agg}} - B(0)) \cdot V_{\mathrm{PEO}}^2 \cdot A_{\mathrm{PEO}}^2(Q) \\ & + 2\Delta\varrho_{\mathrm{C_n}} \cdot \Delta\varrho_{\mathrm{PEO}} \cdot N_{\mathrm{agg}}^2 \cdot V_{\mathrm{C_n}} \cdot V_{\mathrm{PEO}} \cdot A_{\mathrm{C_n}}(Q) \cdot A_{\mathrm{PEO}}(Q) \\ & + V_{\mathrm{PEO}}^2 \cdot \Delta\varrho_{\mathrm{PEO}}^2 \cdot B(Q) \end{aligned} \tag{18}$$

here *Δρ* is the contrast factor i.e. the difference in the scattering length density of the polymer compared to the solvent. The individual scattering amplitudes from the core $A_C(Q)$ and the corona $A_{PEO}(Q)$ are based on assuming a compact homogeneous core density profile, *c* = *constant* (i.e. solvent-free), and a star-like shell density profile, $n_{\mathrm{sh}} \sim r^{-4/3}$, respectively[65]. According to the assumptions, $A_c(Q)$ and $A_{PEO}(Q)$ are weighted by the respective n-alkyl and PEO volumes, V_{Cn} and V_{PEO}, and contrasts $\Delta\rho_{Cn} = \rho_{Cn}-\rho_0$ and $\Delta\rho_{PEO} = \rho_{PEO}-\rho_0$. Here ρ_0 denotes the scattering length density of the solvent. The explicit expressions are given by:

$$A_c(Q) = \frac{3\left(\sin(Q \cdot R_c) - Q \cdot R_c \cos(Q \cdot R_c)\right)}{(Q \cdot R_c)^3} \times e^{-Q^2\,\sigma_{\text{int}}^2/2} \tag{19}$$

$$A_{sh}(Q) = \frac{1}{C}\int_{R_c}^{\infty} \mathrm{d}r\, \frac{4\pi \cdot r^2 \cdot r^{-4/3}}{1 + e^{(r-R_m)/\sigma_m\, R_m}} \cdot \frac{\sin(Q \cdot r)}{Q \cdot r} \times e^{-Q^2\,\sigma_{\text{int}}^2/2} \tag{20}$$

where C is a normalisation constant $\left(C = \int_{R_c}^{\infty} \frac{4\pi \cdot r^2 \cdot r^{-4/3}}{1+\exp^{(r-R_m)/\sigma_m\, R_m}} \mathrm{d}r\right)$

The Gaussian factor in Eq.19 and Eq. 20 accounts for a smooth core-corona interface with σ_{int} as the apparent surface roughness measure. In addition a Fermi cut-off function in Eq. 20 is used in order to terminate the corona. For the analysis σ_m was set to 10% of R_m. *B(Q)* in Eq.18 rationalise the semi-dilute nature of the corona domain. I.e. excluded volume effects inside the shell ("blob-scattering")[66, 67] that can be added incoherently[68] according to:

$$B(Q) = \frac{P_{\text{Beau}}(Q)}{1 + \nu \cdot P_{\text{Beau}}(Q)} \tag{21}$$

here *v* is a parameter describing the effective chain-chain correlations inside the shell. The form factor of interacting self-avoiding chains $P_{Beau}(Q)$ can be empirically modeled by using[69]:

$$P_{\text{Beau}}(Q) = \exp^{-\frac{Q^2\,R_g^2}{3}} + \frac{d_f}{R_g^{d_f}} \cdot \Gamma\left(\frac{d_f}{2}\right) \cdot \left(\frac{\operatorname{erf}\left(\frac{k\,Q\,R_g}{\sqrt{6}}\right)}{Q}\right)^{d_f} \tag{22}$$

where R_g is the radius of gyration of a corona block, d_f is the fractal dimension for a polymer (in a good solvent = 1,7) and *k* is an empirical constant set to 1.06[69]. The R_g of the swollen PEO corona can be roughly estimate by an empiric equation given by Devanand and Selser [70]:

$$R_g = 0.215 \cdot M_w^{0.583} \tag{23}$$

The BAB triblock copolymer causes an effective attractive interaction that brings several micelles together. This results in the formation of larger clusters. The structure factor *S(Q)* is then modelled by points of a random flight model with a step-size *D*:

$$S_N(x) = \frac{2}{1 - \frac{\sin x}{x}} - 1 - \frac{2\left[1 - \left(1 - \frac{\sin x}{x}\right)^N\right]}{N\left(1 - \frac{\sin x}{x}\right)^2}\,\frac{\sin x}{x} \tag{24}$$

where *N* denotes the number of micelles per cluster with $x = Q^*D$ and *D* is the distance

between the cluster centers.

In this way the cluster size N is an integer value. $S_N(Q)$ must be weighted for on-integer values of N. This can easily be done by taking a linear combination of $[N]$ and $[N]+1$ with $p = N - [N]$:

$$S_N(x) = p\, S_{\lfloor N \rfloor} + (1-p)\, S_{\lfloor N \rfloor + 1} \tag{25}$$

here $[N]$ is the largest integer, but not greater than N.

Appendix D: Supplementing SANS results for PCLA-PEG(1000)-PCLA

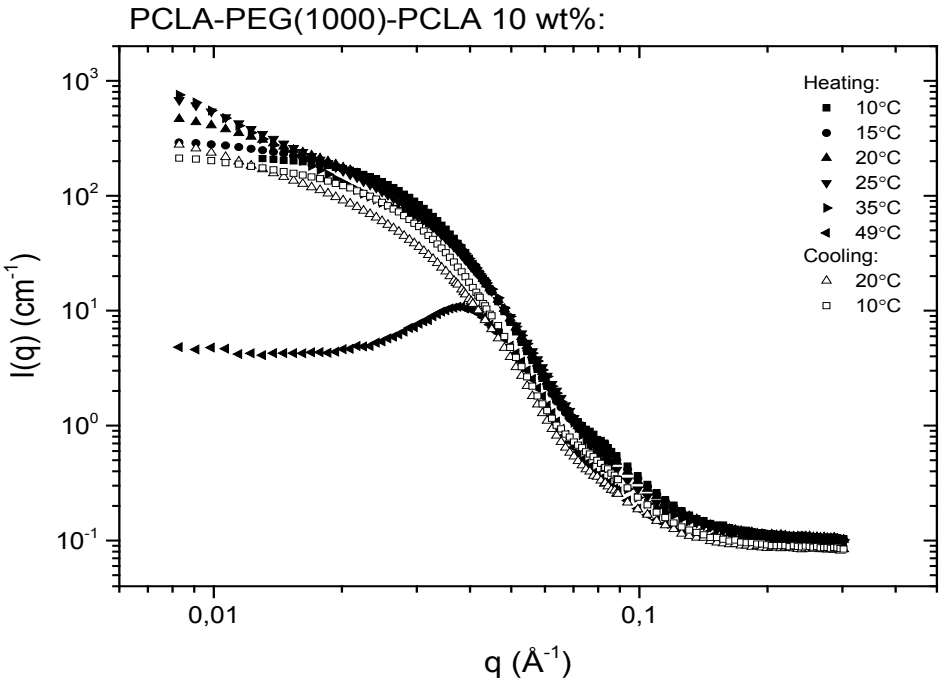

Figure 38. Scattered intensity plotted versus the scattering vector q for a 10 wt% sample of PCLA-PEG(1000)-PCLA.

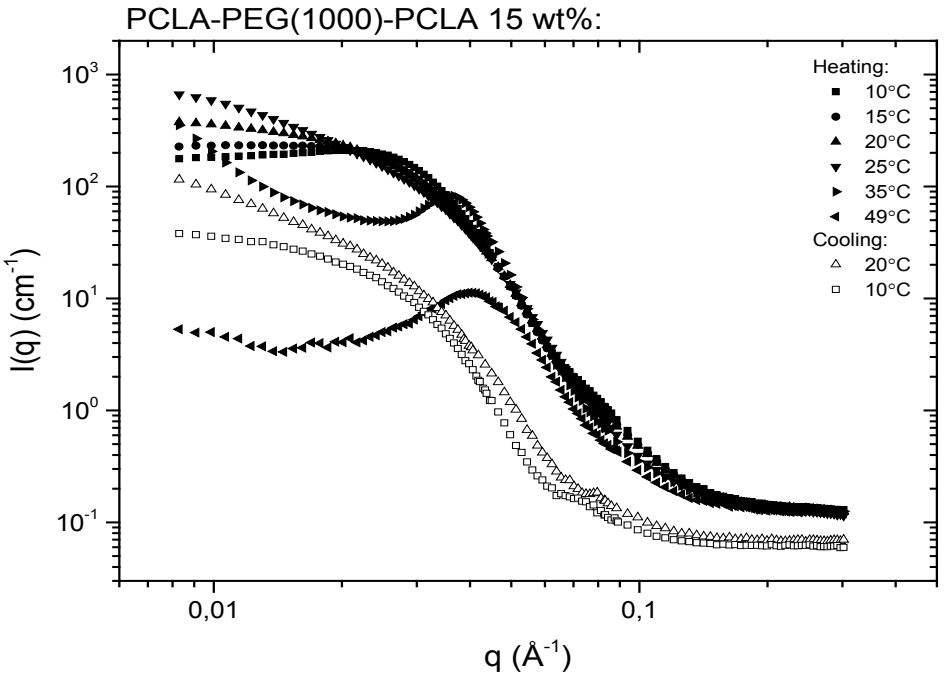

Figure 39. Scattered intensity plotted versus the scattering vector q for a 15 wt% sample of PCLA-PEG(1000)-PCLA.

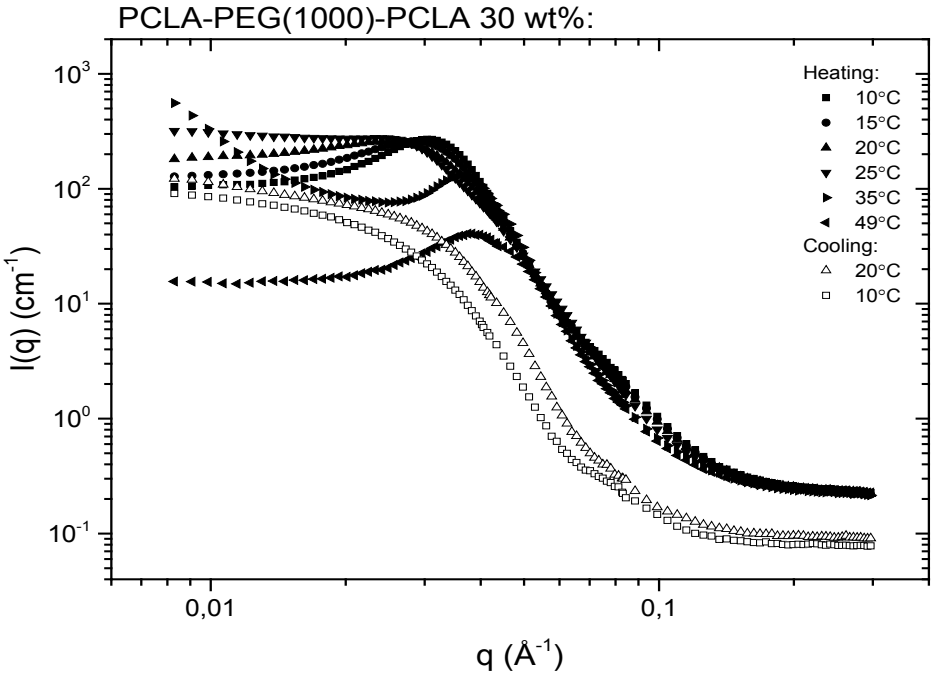

Figure 40. Scattered intensity plotted versus the scattering vector q for a 30 wt% sample of PCLA-PEG(1000)-PCLA.